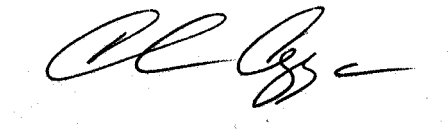Dear Editor Lehtinen,

We have responded to each of the anonymous reviewers comments, as well as those of Dr. Havala Pye. We hope that you find that our responses and revisions adequately address the reviewers concerns. Our responses to the reviewers are provided below, along with a tracked-changes version of our revised manuscript. Please let me know if you require any further information, and we look forward to your decision.

Regards,

Prof. Chris Cappa
University of California, Davis

Response to Interactive comment by H. O. T. Pye on "Simulating Secondary Organic Aerosol in a Regional Air Quality Model Using the Statistical Oxidation Model: 2. Assessing the Influence of Vapor Wall Losses" by C. D. Cappa et al.

Original comments in **black**. Reponses in **blue** and proposed new text is *italicized*.

The Statistical Oxidation Model (SOM) was applied to the South Coast Air Basin (SoCAB) and Eastern US as part of the UCD/CIT regional transport model. The focus was on examining how correcting for vapor wall losses might resolve model/measurement disagreement in terms of SOA magnitude, OC magnitude, and O:C ratios. The SOM model has many nice features, such as the ability to consider wall-loss and fragmentation/functionalization within the chamber fitting procedure as well as explicit predictions of the O:C ratio. The manuscript was well written and easy to follow. My comments are aimed at clarifications.

We thank the commentator for the suggestions as to how to clarify our work. Our responses to specific queries follow below.

Major comments:

1. Make sure that the terms used to characterize simulations as high vs low yield are precisely defined. In this work, high and low refer to the amount of wall loss in the chamber fitting. In Part 1 by Jathar et al., the high and low yield SOM parameterizations refer to low/high NOx regimes. This is potentially confusing to readers trying to follow the evolution of parameters through the literature.

We will clarify the language used, especially expanding figure and table captions to make clear the distinction. Although we understand the potential for misunderstanding, we note that we do use consistent language within each manuscript, and only use the specific terminology SOM-no, SOM-low, and SOM-high to refer to the effects of vapor wall losses, and not for the influence of NO$_x$.

2. Table 1: A correlation coefficient (Pearson's r, concordance correlation coefficient, etc) would be useful for model vs. IMPROVE/STN comparisons. Figure S4-S5 look like the correlation between model and obs might be low.

We do not specifically fit a regression line through the data. Nonetheless, we can calculate the concordance correlation coefficient as:

$$\rho_c = \frac{2s_{xy}}{s_x^2 + s_y^2 + (\bar{x} - \bar{y})^2}$$

where $\bar{x}$ and $\bar{y}$ indicate the mean, s_x^2 and s_y^2 are the variance and s_{xy} is the covariance. We will provide these values in an updated Table 1 (shown below). Indeed, in many cases the values are small (close to zero).

Simulation	NOx parameterization	Southern California						Eastern US					
		STN[a]			IMPROVE[b]			STN[a]			IMPROVE[b,c]		
		Frac. Bias	NMSE	ρ_c	Frac. Bias	NMSE	ρ_c	Frac. Bias	NMSE	ρ_c	Frac. Bias	NMSE	ρ_c
	low	-70	88	0.03	-75	114	0.36	-81	206	0.04	-55	105	0.31
SOM-no	high	-61	69	0.02	-60	85	0.41	-58	166	0.12	-24	84	0.48
	average	-65	78	0.02	-67	97	0.39	-68	180	0.08	-38	89	0.43
	low	-52	64	-0.21	-45	65	0.36	-26	154	0.08	15	85	0.15
SOM-low	high	-39	49	-0.29	-27	47	0.27	-4	171	0.07	38	128	0.10
	average	-45	55	-0.25	-36	54	0.32	-14	160	0.08	28	105	0.12
	low	-25	51	-0.03	-8	46	0.44	26	236	0.15	69	189	0.40
SOM-high	high	-10	38	-0.08	16	43	0.46	45	298	0.15	86	295	0.25
	average	-17	43	-0.05	5	42	0.46	36	265	0.16	79	241	0.31

[a] Observed [OA] for STN sites estimated as $1.6([OC] - 0.5\ \mu g\ m^{-3})$

[b] Observed [OA] for IMPROVE sites estimated as 2.1[OC].

[c] Observed [OA] may be biased low by ~25% in the SE US summer due to evaporation after sampling (Kim et al., 2015).

We will amend the text to state:

> **Error! Reference source not found.** lists statistical metrics of fractional bias, normalized mean square error (NMSE) *and the concordance correlation coefficients* that capture model performance for OA for all simulations for both domains across the STN and IMPROVE monitoring networks. *Fractional bias is calculated as:*
>
> $$Fractional\ bias = \frac{2(C_{OA,sim} - C_{OA,obs})}{C_{OA,sim} + C_{OA,obs}} \tag{1}$$
>
> *and the NMSE as*
>
> $$NMSE = \left| \frac{(C_{OA,sim} - C_{OA,obs})^2}{C_{OA,sim} \times C_{OA,obs}} \right| \tag{2}$$
>
> *where the subscripts sim and obs refer to the simulated and observed OA concentrations, respectively. The concordance correlation coefficients (ρ_c) are calculated as:*
>
> $$\rho_c = \frac{2 s_{sim,obs}}{s_{sim}^2 + s_{obs}^2 + \left(\overline{C_{OA,sim}} - \overline{C_{OA,obs}} \right)^2}$$
>
> *where $\overline{C_{OA,sim}}$ and $\overline{C_{OA,obs}}$ indicate the mean, s_{sim}^2 and s_{obs}^2 are the variance and $s_{sim,obs}$ is the covariance of the simulated and observed OA concentrations.*

3. Simulations for 2010 (coinciding with CalNex) and 2013 (coinciding with SOAS/SEAC4RS) would be useful since concentrations have likely evolved significantly since 2005-2006.

Although we certainly agree with Dr. Pye, such simulations are currently outside the scope of this manuscript.

4. Page 30091: How does SOM overcome the issue of dynamic range if it is based on the same chamber data as an Odum 2-product fit? While Figure S2 seems to show the Odum 2-product fits have some serious errors at lower delta(HC), are those lower delta(HC) constrained by the experimental data?

The "dynamic range" issues arise from the limited number of parameters in the 2-product model, not the data. The SOM overcomes this issue by using a greater number of parameters that span a wider, more continuous volatility range. That said, one can certainly ask the question how well the SOM (or any model) will do at very low concentrations where the measurements are at their limit. Here, we rely on the

structure of the SOM itself, in that the SOM is developed to use a self-consistent set of physically-based rules to describe the chemical evolution of the system. This physical basis to the model provides for greater flexibility and performance at low concentrations (and over a larger dynamic range in general) compared to the 2-product model. We note here also that unpublished comparisons with the GECKO-A model of SOA formation, which is a chemically-explicit model, indicate generally good correspondence between the two models. We will modify the text to read:

> We have determined that this lack of robustness is a result of the limited dynamic range of the 2-product model. *This can be contrasted with the SOM, which includes many more species that span a wider, more continuous volatility range, making it more flexible when fitting the laboratory data.*

5. Page 30095: Is the high or low NOx regime more sensitive to wall-loss corrections? A column could be added to table S1 indicating the SOA yield (for a given set of conditions like total OA, etc.) relative to the uncorrected yield. What if instead of averaging the high/low NOx regime results, the authors only looked at high or low-NOx results? This would allow readers to infer their own SOA enhancements based on the relative dominance of the pathways. It appears that the low-NOx regime may be more sensitive to the wall-loss correction. In SoCAB, the high-NOx pathway is likely to be more relevant. Thus, figure 1 may overestimate the potential impact of wall-loss correction.

Dr. Pye raises an interesting point. How do the R_{wall} values differ between the low-NO_x and high-NO_x simulations? To test this, we have plotted a subset of the R_{wall} values simulated for the eastern US but where the R_{wall} values were not calculated as the ratio between the averaged SOM-high or SOM-low and the SOM-no simulations, but where we have calculated this for each of the NO_x parameterizations individually. (The specific subset selected here corresponds to the data shown in Figure S5 that were compared with the eastern US observations and was chosen because these simulation results were already extracted from the model runs. Given the large number of sites located across the eastern US, and thus corresponding to a wide range of absolute values and conditions, we fully expect that if all of the data from the individual runs were considered, as was done in Fig. 3, similar conclusions would be reached.) Since, as the authors note, the terminology can get confusing, we specifically calculated:

$$R_{wall}(low\ NO_x\ parameterization) = \frac{[SOA]_{lowVWL,lowNO_x}}{[SOA]_{noVWL,lowNO_x}}\ or = \frac{[SOA]_{highVWL,lowNO_x}}{[SOA]_{noVWL,lowNO_x}}$$

and

$$R_{wall}(high\ NO_x\ parameterization) = \frac{[SOA]_{lowVWL,highNO_x}}{[SOA]_{noVWL,highNO_x}}\ or = \frac{[SOA]_{highVWL,highNO_x}}{[SOA]_{noVWL,highNO_x}}$$

and where the subscript "VWL" indicates the vapor wall loss condition and the subscript "NO_x" indicates the NO_x condition. This can be contrasted with what was done in the manuscript, which was:

$$R_{wall}(lowVWL) = \frac{[SOA]_{lowVWL,lowNO_x} + [SOA]_{lowVWL,highNO_x}}{[SOA]_{noVWL,lowNO_x} + [SOA]_{noVWL,highNO_x}}$$

or

$$R_{wall}(highVWL) = \frac{[SOA]_{highVWL,lowNO_x} + [SOA]_{highVWL,highNO_x}}{[SOA]_{noVWL,lowNO_x} + [SOA]_{noVWL,highNO_x}}$$

and where we have again explicitly used "VWL" to indicate the vapor wall loss condition (low or high). It is clear that there is some difference between the simulated R_{wall} values between the low-NO_x and high-NO_x parameterizations, although most points fall close to the one-to-one line. At very low R_{wall} values, the high-NO_x parameterization gives slightly lower R_{wall} than does the low-NO_x parameterization for both the SOM-lowVWL and SOM-highWVL cases. But as the absolute R_{wall} values increase the opposite is true. Regardless, the differences between the NO_x-parameterizations are much smaller than the absolute values of the simulated R_{wall} values. We intend to include this comparison in the revised manuscript, with the figure below added to the supplemental material (along with the equations above) and the following sentence added at P30095, Line 19:

If R_{wall} values are calculated using the simulated SOA concentrations from either the low-NOx or high-NOx parameterizations individually, as opposed to the average values used above, very similar results are obtained (Figure SX).
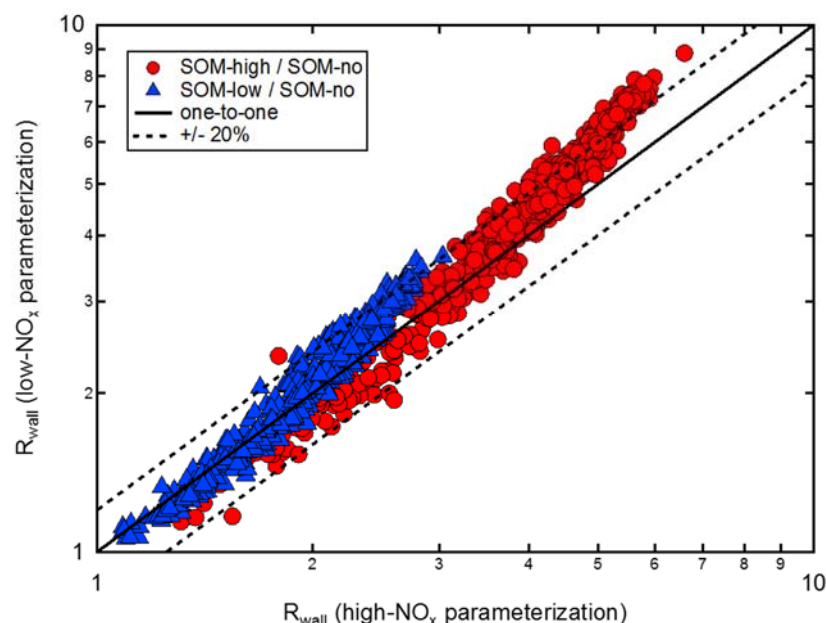
Minor comments:

6. Page 30085, line 10-11: Briefly recap how vapor pressure affects wall loss (decreasing vapor pressure leads to increasing losses?)

We will modify the sentence to read:

Recent observations have demonstrated that organic vapors can be lost to Teflon chamber walls, and that the extent of loss is related to the compound vapor pressures *with lower vapor pressure compounds partitioning more strongly to the walls than higher vapor pressure compounds* (Matsunaga and Ziemann, 2010; Kokkola et al., 2014; Krechmer et al., 2015; Yeh and Ziemann, 2015; Zhang et al., 2015).

7. Page 30088, line 20: Should k_wall and alpha_wall also be mentioned as tunable?

Although these are not tuned in the model here, they are theoretically tunable. However, one should recognize these are coupled, as discussed in Zhang et al. (2014)and shown in their Fig. S4. For the current

study, rather than explicitly tuning k_{wall} (and alpha_wall), we instead consider two specific values of k_{wall}. The reason for this decision is discussed on Page 30089, Section 2.3. To clarify this, we will modify Section 2.3 to state:

> It should be noted that the influence of vapor wall losses is inherent in the fit parameters, and in the absence of walls (i.e. in the atmosphere) the predicted SOA formed will be larger when the fits account for vapor wall losses. *A base case set of parameters with no vapor wall losses assumed during fitting (termed SOM-no) was determined using k_{wall} = 0. In Zhang et al. (2014), an optimal value of k_{wall} = 2 x 10^{-4} s^{-1} was determined for the California Institute of Technology chamber based on simultaneous fitting of the SOM to a set of toluene photooxidation experiments conducted at different seed particle concentrations. Unlike in Zhang et al. (2014), the values of k_{wall} used here were not determined during model fitting. This is because the absolute value of k_{wall} is not well constrained by a single experiment, and the simulations require vapor wall loss corrected parameters for VOCs besides toluene. Therefore, two specific bounding cases that account for vapor wall loss are instead considered based on the results from Zhang et al. (2014).* Specifically, values of k_{wall} = 1 x 10^{-4} s^{-1} and 2.5 x 10^{-4} s^{-1} are considered, corresponding to a low vapor wall loss case (SOM-low) and high vapor wall loss case (SOM-high), respectively.

8. Page 30090, line 6: In which direction is the correction conservative? High or low wall loss?

The question is in reference to the selected value of alpha_particle used in the model, here alpha_particle = 1. We have shown previously (Zhang et al., 2014) that the influence of vapor wall losses is increased when the assumed value of alpha_particle is decreased. Thus, the correction (or really, assumption of alpha_particle = 1) is "conservative" in that it minimizes the influence of vapor wall losses. This is true for both the high and low vapor wall loss cases. But, of course, the use of the larger assumed k_{wall} (i.e. "high" vapor wall loss case) is less conservative than the use of the smaller assumed k_{wall} (i.e. the "low" vapor wall loss case). We will modify the sentence to be:

> Thus, a conservative estimate *that minimizes* the influence of vapor wall losses on SOA formation is obtained using $\alpha_{particle} \geq 0.1$.

9. Page 30092, line 27: May want to mention that the CMAQ POA treatment by Simon and Bhave, although non-volatile, does account for aging of POA along a -1 van Krevlen slope due to OH reaction such that O:C evolves in that atmosphere (with a distinct diurnal profile).

We thank Dr. Pye for pointing out this reference. However, as at this point in the manuscript we are discussing the operation of the SOM model specifically, it does not seem the appropriate location to mention the Simon and Bhave study. It would seem that the addition of such a reference around Page 30103, Line 9/10 would be more appropriate. We will add a reference, in addition to the Murphy et al. (2011) reference.

10. Page 30094, line 1-4: While not always perfectly simulated, we do have some confidence in the ability of models to predict NO:HO2 branching. Models (at fine resolution, perhaps not at 36 km) capture spatial distributions in branching and GEOS-Chem captures seasonal trends in high vs. low-NOx isoprene oxidation products (Kim et al. 2015 ACP). I'm not sure if Carlton et al. 2010 is a good reference here.

We assume that Dr. Pye is referring specifically to the paper "Sources, seasonality, and trends of southeast US aerosol: an integrated analysis of surface, aircraft, and satellite observations with the GEOS-Chem chemical transport model" by Kim et al. (2015), as there is more than one paper in ACP by Kim et al. in

2015. It does not appear that that paper specifically presents NO:HO₂ ratios or compares the simulated NO:HO₂ to observed values. The paper does state "Aerosol chemistry is coupled to HOx -NOx -VOC-O3-BrOx tropospheric chemistry with recent updates to the isoprene oxidation mechanism as described by Mao et al. (2013)," but this does not seem to be a demonstration that the branching is correct. Further, the SOA from isoprene in this paper is "produced with a yield of 3%...formed at the point of emission," and that while they "use four separate tracers in the model to track SOA formed from isoprene and monoterpenes via the high- and low-NO pathways" they also note that "This tracer separation is purely diagnostic as the SOA yields are assumed here to be the same in both pathways". This is not to say that the overall variability in spatial distributions and seasonal trends in branching between low-NO$_x$ and high-NO$_x$ pathways are not well simulated, but it would be great if Dr. Pye were able to point us towards a reference that more directly addresses this issue (or let us know if we are looking at the wrong reference).

11. Page 30096, line 1: This line reads that there is more absolute SOA over the ocean than land. Is that what was intended?

No, this is not what was intended. This was stated backwards. It should instead read: "Indeed, the ratio between the predicted average SOA *in downtown LA (urban) to that over the Pacific Ocean near the coast of LA (regional)* and decreases from 2.3 (SOM-no) to 1.5 (SOM-low) to 1.3 (SOM-high), for example." We thank Dr. Pye for catching this error.

12. Page 30096, line 17-18, the authors may want to restrict the fSOA enhancements here to values from the Riverside or LA-Basin locations as higher ratios correspond to low absolute OA values.

We appreciate the suggestion and will add more specific values during revision. Inspection of Fig. 3 indicates that the SOM-no, SOM-low and SOM-high f_{SOA} values in Riverside are ~0.2, ~0.35 and 0.5, respectively.

13. Page 30099, was there an overall model bias in CO?

Yes, it would appear that the simulated CO is biased slightly high. As stated, the simulated background [CO] = 130 ppb while the observed background [CO] ~ 105 ppb.

14. Page 30100: Keep in mind that NOx has changed significantly from 2005-2013 (e.g. Russell et al. 2012 ACP) and that would affect the IEPOX-OA abundance. Changes in sulfate/acidity would also affect IEPOX-OA (e.g. Pye et al. 2013, Marais et al. 2015 ACPD).

We thank Dr. Pye for pointing these issues out. We will revise the manuscript to note these points in the context of the model/measurement comparison across years. Specifically, we intend to add the sentence:

Additionally, it should be kept in mind that the ambient NO$_x$ concentrations in SoCAB have decreased substantially from 2005-2013 (Russell et al., 2012).

15. Page 30102: The fraction fossil discussion that compares 2005 simulations to 2010 field data may need more caveats in its current form (ie highlighting potential changes in fossil fraction from 2005 to 2013). Could the authors not estimate the fraction fossil of SOC in the model given that the O:C ratio is known for the model species? That may eliminate some of the discrepancy in comparison.

Dr. Pye raises a good point, that the carbon mass can be estimated from the SOA mass and the species-specific O:C values, which can then be used to calculate a carbon-specific fossil fraction. Specifically, the mass concentration of carbon (C_C) is related to the mass concenration of SOA (C_{SOA}) as:

$$C_C = \frac{C_{SOA}}{O:C + 1}$$

We have used the above equation to calculate C_C values for each SOA type, and from this the carbon-specific fossil fractions (F_{SOC}). We find that the calculated fossil fractions generally change by a small amount. In some cases the carbon-specific fossil fraction is larger than the SOA fossil fraction and in others it is smaller. The average absolute difference for SoCAB is 0.00 and for the eastern US is 0.02. The calculated F_{SOA} and F_{SOC} values for the low- and high-NO_x simulations for the three vapor wall loss cases (SOM-no, SOM-low and SOM-high) are compared in the table below. We will add this table to the supplemental material and include the following in the main text on Page 30102:

> The fossil fraction of secondary organic carbon can be calculated from the simulated SOA concentrations by accounting for the differences in the O:C atomic ratios of the different SOA types to facilitate more direct comparison between the simulations and observations. Specifically, the carbon mass concentration (C_C) is related to the SOA mass concentration (C_{SOA}) for a given SOA type through the relationship:

$$C_C = \frac{C_{SOA}}{O:C+1} \qquad (1)$$

> The O:C values of the different SOA types are not constant in the SOM due to the continuous evolution of the product distribution. However, for a given SOA type the simulated O:C values vary over a narrow range (Cappa et al., 2013) and thus an average value can be used. The resulting $F_{SOC,fossil}$ values are compared with the $F_{SOA,fossil}$ values in Table S2 and are found to be very similar.

Vapor Wall Loss Case	NO_x condition	Central LA		Riverside	
		SOA	SOC	SOA	SOC
SOM-no	high-NO_x	0.27	0.25	0.28	0.25
	low-NO_x	0.44	0.41	0.40	0.37
SOM-low	high-NO_x	0.22	0.23	0.27	0.28
	low-NO_x	0.32	0.30	0.35	0.33
SOM-high	high-NO_x	0.22	0.25	0.28	0.31
	low-NO_x	0.33	0.32	0.37	0.36
		Atlanta		Smokey Mountains	
		SOA	SOC	SOA	SOC
SOM-no	high-NO_x	0.10	0.08	0.14	0.12
	low-NO_x	0.17	0.15	0.15	0.13
SOM-low	high-NO_x	0.19	0.18	0.27	0.27
	low-NO_x	0.18	0.17	0.22	0.21
SOM-high	high-NO_x	0.25	0.27	0.32	0.35
	low-NO_x	0.20	0.19	0.24	0.23

16. Table S1 seems to indicate monoterpenes and sesquiterpenes have the same SOA yield. Why was that decision made?

The values in Table S1 do not indicate that the monoterpenes and sesquiterpenes have the same SOA yields. We assume that the SOM parameters that describe the SOA formation are the same. The sesquiterpenes have a greater number of carbon atoms than the monoterpenes. Consequently, the sesquiterpenes have a larger SOA yield than the monoterpenes because the oxidation products from sesquiterpene oxidation have lower volatility. We will clarify this aspect by adding the following to Table S1:

> [+]*Although the same set of parameters are used to describe the formation of oxidation products and SOA from monoterpenes and sesquiterpenes, the SOA yield from sesquiterpenes is larger than for monoterpenes due to the larger number of carbon atoms comprising sesquiterpenes.*

17. What oxidants (OH, O3, NO3?) are considered for SOA purposes?

In the SOM we consider reactions with OH, O_3 and NO_3, although make particular simplifications for computational efficiency. In particular, each precursor VOC is allowed to react with either OH, O_3 or NO_3 as characterized by an oxidant-specific rate coefficient. However, the products and product distributions of the first-generation products are assumed to be oxidant independent. This simplification is identical to that employed in CMAQv4.7 (Carlton et al., 2010). Reactions of subsequent oxidized SOM products then occur only via reaction with OH radicals according to the SOM parameterization associated with that precursor VOC (as determined by fitting photooxidation experiments). Reactions with O_3 and NO_3 will be most important for the mono- and sesquiterpenes. We will add the following information in the section 3.5 Model Simulations and Outputs:

> *Each precursor VOC is allowed to react with either OH, O_3 or NO_3 as characterized by an oxidant-specific rate coefficient, although the products and product distributions of the first-generation products are assumed to be oxidant independent. This simplification is identical to that employed in CMAQv4.7 (Carlton et al., 2010). Reactions of subsequent oxidized SOM products then occur only via reaction with OH radicals according to the SOM parameterization associated with that precursor VOC (as determined by fitting the photooxidation experiments).*

18. Figure 5: I'm surprised the base (SOM-no) simulation gets such high OA/CO ratios. In our CMAQ and CMAQ-VBS simulations (Woody et al. 20105 ACPD), we see slopes of 8 and 66 ug/m3/ppm compared to 108 in the observations for SOA/del(CO) vs. log(NOx/NOy).

The reported OA/ΔCO ratio for the SOM-no simulation was 23 μg m^{-3} ppm^{-1}. Certainly this is larger than the 8 μg m^{-3} ppm^{-1} reported by Woody et al. for their standard CMAQ simulation, but it is lower than the 66 μg m^{-3} ppm^{-1} reported for their CMAQ-VBS simulation. It is difficult to intuit the reason for this difference between models. It is possible that it arises from the difference in datasets used to develop the SOM parameterization as compared to the 2-product and VBS parameterizations used in Woody et al. (2015), although we note that the results in Jathar et al. (2015b) (which focus on the performance of SOM-no compared to other model formulations) suggest that minimal differences between simulations should be obtained due to this difference. It is possible that the difference is due to the different simulation periods and specific locations, although this seems relatively unlikely. Although establishing the exact reason for such a difference in the base model performance would certainly be of interest, it is outside of the scope of the current study.

19. Provide an estimate of the amount of computer processing time required for a SOM vs. base simulation.

To quote from Jathar et al. (2015a),

All simulations were performed for both domains: SoCAB and the eastern US. The simulations were performed on a computer cluster operated and maintained at the University of California, Davis. Each simulation was performed using Intel Core i5-3570s for a total of 40 core processors and shared memory of 40 GB. The simulations were performed for 19 days with the first 5 days used for spin up. For the SoCAB, each simulated day required approximately 4 h of elapsed time so a 19-day episode was simulated in less than 4 days. For the eastern US, each simulated day required approximately 9 h of elapsed time so a 19-day episode was simulated in about 8 days.

These numbers can be compared with simulations run using the 2-product "Base" model in Jathar et al. (2015b). These "Base" simulations took on average about 30 hours for a 19 day episode in the SoCAB, or 1.6 h per day, so ran faster by a factor of 2.5. However, the base model was run using 16 size sections as compared to the 8 used with the SOM, and thus the actual difference was smaller most likely by somewhere around a factor of 2. We will add the following sentence at the end of Section 3.2:

The use of the SOM to represent SOA formation leads to an increase of about a factor of 2.5 or less in computer processing time required compared to use of the 2-product model.

References

Cappa, C. D., Zhang, X., Loza, C. L., Craven, J. S., Yee, L. D., and Seinfeld, J. H.: Application of the Statistical Oxidation Model (SOM) to secondary organic aerosol formation from photooxidation of C12 Alkanes, Atmos. Chem. Phys., 13, 1591-1606, doi:10.5194/acp-13-1591-2013, 2013.

Carlton, A. G., Bhave, P. V., Napelenok, S. L., Edney, E. O., Sarwar, G., Pinder, R. W., Pouliot, G. A., and Houyoux, M.: Model Representation of Secondary Organic Aerosol in CMAQv4.7, Environ. Sci. Technol., 44, 8553-8560, doi:10.1021/es100636q, 2010.

Jathar, S. H., Cappa, C. D., Wexler, A. S., Seinfeld, J. H., and Kleeman, M. J.: Multi-generational Oxidation Model to Simulate Secondary Organic Aerosol in a 3D Air Quality Model, Geosci. Model Dev., 8, 2553-2567, doi:10.5194/gmd-8-2553-2015, 2015a.

Jathar, S. H., Cappa, C. D., Wexler, A. S., Seinfeld, J. H., and Kleeman, M. J.: Simulating secondary organic aerosol in a regional air quality model using the statistical oxidation model – Part 1: Assessing the influence of constrained multi-generational ageing, Atmos. Chem. Phys. Discuss., 15, 25837-25872, doi:10.5194/acpd-15-25837-2015, 2015b.

Kim, P. S., Jacob, D. J., Fisher, J. A., Travis, K., Yu, K., Zhu, L., Yantosca, R. M., Sulprizio, M. P., Jimenez, J. L., Campuzano-Jost, P., Froyd, K. D., Liao, J., Hair, J. W., Fenn, M. A., Butler, C. F., Wagner, N. L., Gordon, T. D., Welti, A., Wennberg, P. O., Crounse, J. D., St. Clair, J. M., Teng, A. P., Millet, D. B., Schwarz, J. P., Markovic, M. Z., and Perring, A. E.: Sources, seasonality, and trends of southeast US aerosol: an integrated analysis of surface, aircraft, and satellite observations with the GEOS-Chem chemical transport model, Atmos. Chem. Phys., 15, 10411-10433, doi:10.5194/acp-15-10411-2015, 2015.

Kokkola, H., Yli-Pirilä, P., Vesterinen, M., Korhonen, H., Keskinen, H., Romakkaniemi, S., Hao, L., Kortelainen, A., Joutsensaari, J., Worsnop, D. R., Virtanen, A., and Lehtinen, K. E. J.: The role of low volatile organics on secondary organic aerosol formation, Atmos. Chem. Phys., 14, 1689-1700, doi:10.5194/acp-14-1689-2014, 2014.

Krechmer, J. E., Coggon, M. M., Massoli, P., Nguyen, T. B., Crounse, J. D., Hu, W., Day, D. A., Tyndall, G. S., Henze, D. K., Rivera-Rios, J. C., Nowak, J. B., Kimmel, J. R., Mauldin, R. L., Stark, H., Jayne, J. T., Sipilä, M., Junninen, H., Clair, J. M. S., Zhang, X., Feiner, P. A., Zhang, L., Miller, D. O., Brune, W. H., Keutsch, F. N., Wennberg, P. O., Seinfeld, J. H., Worsnop, D. R., Jimenez, J. L., and Canagaratna, M. R.: Formation of Low Volatility Organic Compounds and Secondary Organic Aerosol from Isoprene Hydroxyhydroperoxide Low-NO Oxidation, Environ. Sci. Technol., 49, 10330-10339, doi:10.1021/acs.est.5b02031, 2015.

Matsunaga, A. and Ziemann, P. J.: Gas-Wall Partitioning of Organic Compounds in a Teflon Film Chamber and Potential Effects on Reaction Product and Aerosol Yield Measurements, Aerosol Sci. Technol., 44, 881-892, doi:10.1080/02786826.2010.501044, 2010.

Murphy, B. N., Donahue, N. M., Fountoukis, C., and Pandis, S. N.: Simulating the oxygen content of ambient organic aerosol with the 2D volatility basis set, Atmos. Chem. Phys., 11, 7859-7873, doi:10.5194/acp-11-7859-2011, 2011.

Russell, A. R., Valin, L. C., and Cohen, R. C.: Trends in OMI NO2 observations over the United States: effects of emission control technology and the economic recession, Atmos. Chem. Phys., 12, 12197-12209, doi:10.5194/acp-12-12197-2012, 2012.

Woody, M. C., Baker, K. R., Hayes, P. L., Jimenez, J. L., Koo, B., and Pye, H. O. T.: Understanding sources of organic aerosol during CalNex-2010 using the CMAQ-VBS, Atmos. Chem. Phys. Discuss., 15, 26745-26793, doi:10.5194/acpd-15-26745-2015, 2015.

Yeh, G. K. and Ziemann, P. J.: Gas-wall partitioning of oxygenated organic compounds: Measurements, structure-activity relationships, and correlation with gas chromatographic retention factor, Aerosol Sci. Technol., 49, 727-738, doi:10.1080/02786826.2015.1068427, 2015.

Zhang, X., Cappa, C. D., Jathar, S. H., McVay, R. C., Ensberg, J. J., Kleeman, M. J., and Seinfeld, J. H.: Influence of vapor wall loss in laboratory chambers on yields of secondary organic aerosol, Proc. Nat. Acad. Sci., 111, 5802-5807, doi:10.1073/pnas.1404727111, 2014.

Zhang, X., Schwantes, R. H., McVay, R. C., Lignell, H., Coggon, M. M., Flagan, R. C., and Seinfeld, J. H.: Vapor wall deposition in Teflon chambers, Atmos. Chem. Phys., 15, 4197-4214, doi:10.5194/acp-15-4197-2015, 2015.

Correction to our Response to Interactive comment by H. O. T. Pye on "Simulating Secondary Organic Aerosol in a Regional Air Quality Model Using the Statistical Oxidation Model: 2. Assessing the Influence of Vapor Wall Losses" by C. D. Cappa et al.

An incorrect equation for converting from secondary organic aerosol (SOA) to secondary organic carbon (SOC) mass concentrations was previously given. The correct equation is:

$$C_{SOC} = C_{SOA} \cdot \frac{N_C \cdot MW_C}{MW_{SOA}} = \frac{N_C \cdot MW_C}{N_C \cdot MW_C + N_O \cdot MW_O + N_H \cdot MW_H} = \frac{C_{SOA}}{\frac{4}{3}(O{:}C) + \frac{1}{12}(H{:}C) + 1}$$

where MW_C, MW_O, MW_H are the molecular weights and N_C, N_O, and N_H the number of carbon, oxygen and hydrogen atoms, respectively. This makes no difference to the conclusions reached.

Response to Interactive comment by Reviewer #1 on "Simulating Secondary Organic Aerosol in a Regional Air Quality Model Using the Statistical Oxidation Model: 2. Assessing the Influence of Vapor Wall Losses" by C. D. Cappa et al.

Original comments in **black**. Reponses in **blue** and proposed new text is *italicized*.

The authors have evaluated the performance of the Statistical Oxidation Model (SOM) within the UCD/CIT regional model for the South Coast Air Basin and Eastern US. The version of SOM used here was fit to laboratory chamber data after accounting for vapor wall losses. Low and high values of wall loss rates were considered to approximately account for the uncertainty in this process. Predicted SOA mass concentrations using the "high wall loss" fits are found to be in much better agreement with observations compared to "no wall loss" and "low wall loss" fits. The results are very interesting, the paper is well written and is recommended for publication in ACP after addressing the following comments.

We thank the reviewer for the comments, and address them each in turn below.

(1) The dependence of SOA yields on pre-existing aerosol surface area in the chamber makes it is clear that vapor wall loss must be accounted in the interpretation of laboratory chamber data. However, it is not clear how the exercise of accounting for vapor wall loss yields a unique set of fitted values for k_wall, gas-phase yields of species with different volatilities (C*), etc.

It is important to clarify here that the k_{wall} values used in this work were not derived as part of this work: the determination of k_{wall} values that are reasonable and appropriate for the Caltech chamber is discussed extensively in [*Zhang et al.*, 2014]. In *Zhang et al.* [2014], an optimal value of k_{wall} was determined via simultaneous fitting of SOA formation experiments performed using different seed aerosol concentrations but with all other experimental conditions held constant. This exercise resulted in an optimal value of 2.5 x 10^{-4} s^{-1}. This is equal to the "high" wall loss case used here. The "low" case was selected as a reasonable lower value to examine the sensitivity of the results to use of a lower k_{wall} value, i.e. to slower vapor wall loss. In Zhang et al. [2014], unique sets of SOM parameters (the fragmentation and functionalization parameters and the volatility decrease per oxygen atom added) were obtained for each k_{wall} assumed. In other words, the specific model parameters ("fitted values") are specific to an assumed k_{wall} value. We have aimed to clarify this in the revised manuscript. Specifically, we have added the following in Section 3.3.1 (new text in italics):

"*A base case set of parameters with no vapor wall losses assumed during fitting (termed SOM-no) was determined using k$_{wall}$ = 0. In Zhang et al. [2014], an optimal value of k$_{wall}$ = 2 x 10^{-4} s^{-1} was determined for the California Institute of Technology chamber based on simultaneous fitting of the SOM to a set of toluene photooxidation experiments conducted at different seed particle concentrations. Unlike in Zhang et al. (2014), the values of k$_{wall}$ used here were not determined during model fitting. This is because the absolute value of k$_{wall}$ is not well constrained by a single experiment, and the simulations require vapor wall loss corrected parameters for VOCs besides toluene. Therefore, two specific bounding cases that account for vapor wall loss are instead considered based on the results from Zhang et al. (2014). Specifically, values of k$_{wall}$ = 1 x 10^{-4} s^{-1} and 2.5 x 10^{-4} s^{-1} are considered, corresponding to a low vapor wall loss case (SOM-low) and high vapor wall loss case (SOM-high), respectively.*"

(2) Were the model fittings done at the end of each chamber experiment or as a function of time in a given experiment?

The model was fit as a function of time, as described in Zhang et al. [2014] and *Cappa et al.* [2013]. The SOM fits are not simply end of experiment fits. We have clarified this point in the current manuscript as follows (new text in italics):

In Section 3.2: "The parameters used in the current work have been determined by fitting to *time-dependent* data from SOA formation experiments conducted in the Caltech chamber both with and without accounting for vapor wall losses during the fitting process (discussed further below)."

and

In Section 3.3.1: "SOM was fit to *time-dependent* SOA formation experiments conducted in the California Institute of Technology chamber, following the methodologies described in *Cappa et al.* [2013] and *Zhang et al.* [2014]."

(3) It is stated that mass accommodation coefficient (alpha_particle) was assumed equal to 1. This indeed seems too conservative, especially if the SOA particles are semisolid and the gas-particle partitioning timescale is longer than currently assumed. If the chamber experiments were conducted under low RH then it is likely that the SOA particles were viscous semisolids. Please state the RH at which the fits were done and comment on how might the results change if alpha_particles < 0.1.

The reviewer raises a good point. All experiments were done at low (<10%) relative humidity. And, in fact, in *Zhang et al.* [2014] we found that the effective mass accommodation coefficient was < 0.1 (specifically, ~1-2 x 10^{-3}). As was shown in that work, if the same k_{wall} is used (i.e. k_{wall} = 2.5 x 10^{-4} s^{-1}) but $\alpha_{particle}$ was instead assumed = 1 (i.e. instantaneous partitioning), the magnitude of influence of vapor wall losses on the SOA may be less than or similar to when a smaller $\alpha_{particle}$ is assumed. In other words, it is not straightforward to quantitatively understand the impact of the $\alpha_{particle}$ = 1 assumption used here compared to if some smaller $\alpha_{particle}$ had been used. Nonetheless, in all likelihood had a smaller $\alpha_{particle}$ been assumed then the impact of accounting for vapor wall losses on the simulated SOA concentrations would likely have been as large or larger. We now address this point in the conclusions through the addition of the following (new text in italics):

"Overall, the generally improved model performance when vapor wall losses are accounted for—in terms of both absolute and relative concentrations and in terms of SOA properties—suggests that accounting for this chamber effect in atmospheric simulations of SOA is important, although certainly requiring further examination. *For example, it was assumed here that the gas-particle mass accommodation coefficient was unity; had smaller values of $\alpha_{particle}$ been assumed during development of the SOM parameterizations used here it is likely that the increase in the simulated SOA concentration when vapor wall losses were accounted for would have increased for a given k_{wall} [Zhang et al., 2014].* Our results qualitatively agree with other recent efforts to assess the influence of vapor wall losses on ambient SOA concentrations [*Baker et al.*, 2015; *Hayes et al.*, 2015], but as our accounting for vapor wall loss is inherent in the SOA parameterization the simulations here serve to provide a more robust assessment."

A similar question was raised by Reviewer #2, and we refer the reader to our Response to Point 2 to Reviewer #2 for additional discussion.

Baker, K. R., A. G. Carlton, T. E. Kleindienst, J. H. Offenberg, M. R. Beaver, D. R. Gentner, A. H. Goldstein, P. L. Hayes, J. L. Jimenez, J. B. Gilman, J. A. de Gouw, M. C. Woody, H. O. T. Pye, J. T. Kelly, M. Lewandowski, M. Jaoui, P. S. Stevens, W. H. Brune, Y. H. Lin, C. L. Rubitschun, and J. D. Surratt (2015), Gas and aerosol carbon in California: comparison of measurements and model predictions in Pasadena and Bakersfield, *Atmos. Chem. Phys.*, *15*, 5243-5258.

Cappa, C. D., X. Zhang, C. L. Loza, J. S. Craven, L. D. Yee, and J. H. Seinfeld (2013), Application of the Statistical Oxidation Model (SOM) to secondary organic aerosol formation from photooxidation of C12 Alkanes, *Atmos. Chem. Phys.*, *13*, 1591-1606.

Hayes, P. L., A. G. Carlton, K. R. Baker, R. Ahmadov, R. A. Washenfelder, S. Alvarez, B. Rappenglück, J. B. Gilman, W. C. Kuster, J. A. de Gouw, P. Zotter, A. S. H. Prévôt, S. Szidat, T. E. Kleindienst, J. H. Offenberg, and J. L. Jimenez (2015), Modeling the formation and aging of secondary organic aerosols in Los Angeles during CalNex 2010, *Atmos. Chem. Phys.*, *15*, 5773-5801.

Zhang, X., C. D. Cappa, S. H. Jathar, R. C. McVay, J. J. Ensberg, M. J. Kleeman, and J. H. Seinfeld (2014), Influence of vapor wall loss in laboratory chambers on yields of secondary organic aerosol, *Proc. Nat. Acad. Sci.*, *111*(16), 5802-5807.

Response to Interactive comment by Anonymous Reviewer 2

Original comments in **black**. Reponses in **blue** and proposed new text is *italicized*.

The manuscript "Simulating secondary organic aerosol in a regional air quality model using the statistical oxidation model – Part 2: Assessing the influence of vapor wall losses" by Cappa et al presents a study of how wall-losses of secondary organic aerosol (SOA) in chamber measurements affect the modeled atmospheric SOA concentrations. There have been several studies on wall losses in chamber measurements. However, to my knowledge this is the first study that has comprehensively taken chamber wall losses into account in a large scale atmospheric model. The manuscript fits well in the scope of Atmospheric Chemistry and Physics and very well written. I can recommend it to be published after the following minor issues have been addressed:

We thank the reviewer for the comments. Our responses to specific queries follow below.

1. Abstract, Page 30083, Line 28, "Similar improvements...": This sentence is difficult to understand without reading the whole manuscript. In addition, in Section 2.3.2 it is said that with more volatility bins, "wall-less" fits could be determined. Although the results of this study strongly indicate that wall-losses have to be taken into account in order to reproduce observed SOA properties, I would recommend excluding this sentence from the Abstract.

We agree that this sentence may be difficult to understand without the context of the entire manuscript, and will delete this sentence in the abstract upon revision.

2. Page 30089, Line 25-: Doesn't the accommodation coefficient have any effect on the amount of SOA or is the effect insignificant?

The accommodation coefficient can influence the simulated amount of SOA. However, if the original parameterization was developed using the same accommodation coefficient as is used in the 3D model, then much of the effect will inherently be accounted for. Consider that in (Zhang et al., 2014) we found it was possible to fit laboratory data for individual experiments with good fidelity using a range of accommodation coefficients by altering the other model parameters to account for the variation in the net accommodation rate. If, however, one were to develop a parameterization using a particular value of the accommodation coefficient but then were to perform simulations using a different value then certainly the simulated SOA concentration would be dramatically influenced. In the current work, we have developed the parameterization using the same accommodation coefficient as is used in the 3D simulations, and thus we do not expect that the accommodation coefficient would directly influence the amount of SOA simulated in the model. There is, however, an indirect effect in that an assumption of smaller accommodation coefficients during the parameterization development (i.e. during data fitting) leads to a larger influence of vapor wall losses (McVay et al., 2014; Zhang et al., 2014). As noted on P30090, Line 5 (and discussed further in our response to Dr. Pye), we assume that the gas-particle accommodation coefficient is unity here, and thus these simulations represent a conservative estimate (likely lower estimate for a given assumed k_{wall}) of the influence of vapor wall losses on the simulated absolute SOA concentrations. A similar question was raised by Reviewer #1, and we refer the reader to our Response to Point 3 to Reviewer #1 for additional discussion.

3. Page 30091, Line 11: This inconsistent behaviour should be explained. Now it is only shown in Fig S2 and not really explained anywhere.

We will elaborate on this idea. More specifically, by "inconsistent behavior" we mean that some fits were "good," some were "okay" and some were quite obviously "poor." These are of course qualitative statements, although do convey the point shown in Fig. S2. We will modify the specific sentence to read:

> Thus, when fits were performed, inconsistent behavior between the different vapor wall loss conditions was obtained over the atmospherically relevant concentration range (~ 0.1–20 µg m^{-3}) *in that some of the fits matched the data well over the entire range while other fits deviated strongly from the observations, especially at lower SOA concentrations.*

4. Page 30093, Line 29: How is SOA formation from isoprene a notable exception?

By "notable exception" we mean that the HO$_2$/NO dependence of the SOA yields has been explored in detail for this system. To clarify our point, we will modify the sentence to read:

> (SOA formation from isoprene is a notable exception *in that the dependence of SOA formation on HO$_2$ and NO has been examined in detail* (e.g. Xu et al., 2014).)

5. Page 30095, Line 26: Should this be along the lines of "R_{wall} increases with decreasing SOA concentration"?

Yes, we can modify the sentence as suggested to make it clearer.

6. Page 30096, Lines 4-7: Is this true for both relative and absolute differences? I would expect that the absolute differences in concentrations between the wallloss and no-wall-loss simulations are higher in high-source regions.

We agree with the reviewer that the absolute differences are likely to be larger where the absolute concentrations are larger. Our focus is more on the relative difference, or more specifically the relative model/measurement difference. We will modify the sentence to read:

> Additionally, it has been suggested that the typical underprediction of SOA by air quality and chemical transport models *relative to observations* might increase with photochemical age (Volkamer et al., 2006). The current results suggest the possibility that the SOA concentrations in more remote (lower concentration) regions may be underestimated in models to a greater extent *in a relative sense* than in high-source (higher concentration) regions due to a lack of accounting for vapor wall losses, *although the absolute differences in SOA concentrations may be larger in regions where absolute concentrations are larger*.

7. Page 30102, Line 1: It is unclear to me, what is the "fossil fraction of SOA".

The fossil fraction of SOA is the fraction of the total SOA that is sourced from fossil-derived VOCs (e.g. toluene, alkanes) as opposed to biogenic VOCs (e.g. isoprene, monoterpenes, sesquiterpenes). We will state this more explicitly as:

> There are some changes in the anthropogenic fraction of SOA when vapor wall losses are accounted for. *The anthropogenic fraction of SOA is defined here as the sum of the SOA from long alkanes and aromatics, which are emitted from combustion of fossil fuels, divided by the sum of the SOA from isoprene, monoterpenes and sesquiterpenes, which are emitted by trees, plants and other natural sources. The ^{14}C isotopic signature of fossil-derived VOCs is different from that of biogenically derived*

VOCs, and thus their respective contributions to SOA can be partially constrained via experimental analysis of the ^{14}C content of OA (Zotter et al., 2014). We assume the anthropogenic fraction is equivalent to the fossil fraction of SOA (termed $F_{SOA,fossil}$).

8. Page 30105: Since the diurnal variation of NOx concentrations haven't been taken into account in these simulations, would you expect the model to reproduce diurnal profiles well?

This question is in reference to the diurnal behavior of the O:C values that are discussed on Page 30105. The O:C of SOA shows only a minor dependence on the NO_x condition (Chhabra et al., 2010; Chhabra et al., 2011; Cappa et al., 2013), and thus we expect that the simulations are able to capture the general diurnal variations, which are driven mostly by diurnal changes in the particular SOA source and the POA contribution, even though the NO_x variability is not explicitly accounted for. However, since the absolute amount of SOA varies between the NO_x parameterizations, the SOA/OA ratio will differ between the low-NO_x and high-NO_x parameterizations for a given vapor wall loss condition (SOM-no, SOM-low or SOM-high). This could in turn influence the simulated O:C. Therefore, we have extracted the O:C ratios for the different NO_x parameterizations for each vapor wall loss condition and compared them to the average values, which are shown in the manuscript. The figure below shows the results of this exercise. It is apparent that the O:C differs only be a minor amount between the different NO_x parameterizations for a given vapor wall loss condition. The much larger influence comes from the different vapor wall loss parameterizations. Therefore, we can conclude that to a large extent not having accounted explicitly for diurnal variations in NO_x have minimal influence on the conclusions regarding the atomic ratios. We will add the following sentence to the manuscript:

The simulated diurnal profiles for a given vapor wall loss condition exhibit only very minor differences between the different NO_x parameterizations, with the high-NO_x parameterization giving a slightly higher O:C than the low-NO_x parameterization.
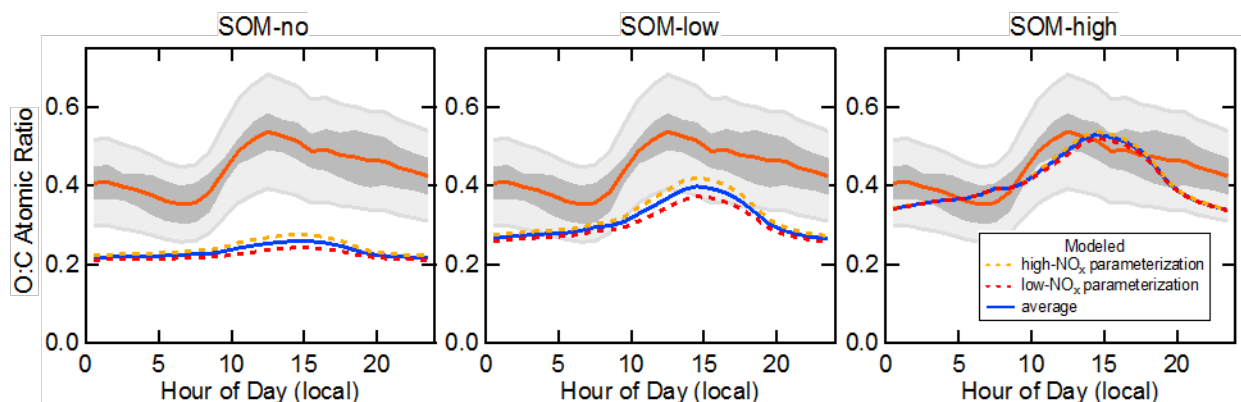
References

Cappa, C. D., Zhang, X., Loza, C. L., Craven, J. S., Yee, L. D., and Seinfeld, J. H.: Application of the Statistical Oxidation Model (SOM) to secondary organic aerosol formation from photooxidation of C12 Alkanes, Atmos. Chem. Phys., 13, 1591-1606, doi:10.5194/acp-13-1591-2013, 2013.

Chhabra, P. S., Flagan, R. C., and Seinfeld, J. H.: Elemental analysis of chamber organic aerosol using an aerodyne high-resolution aerosol mass spectrometer, Atmos. Chem. Phys., 10, 4111-4131, doi:10.5194/acp-10-4111-2010, 2010.

Chhabra, P. S., Ng, N. L., Canagaratna, M. R., Corrigan, A. L., Russell, L. M., Worsnop, D. R., Flagan, R. C., and Seinfeld, J. H.: Elemental composition and oxidation of chamber organic aerosol, Atmos. Chem. Phys., 11, 8827-8845, doi:10.5194/acp-11-8827-2011, 2011.

McVay, R. C., Cappa, C. D., and Seinfeld, J. H.: Vapor–Wall Deposition in Chambers: Theoretical Considerations, Environ. Sci. Technol., 48, 10251-10258, doi:10.1021/es502170j, 2014.

Xu, L., Kollman, M. S., Song, C., Shilling, J. E., and Ng, N. L.: Effects of NOx on the Volatility of Secondary Organic Aerosol from Isoprene Photooxidation, Environ. Sci. Technol., 48, 2253-2262, doi:10.1021/es404842g, 2014.

Zhang, X., Cappa, C. D., Jathar, S. H., McVay, R. C., Ensberg, J. J., Kleeman, M. J., and Seinfeld, J. H.: Influence of vapor wall loss in laboratory chambers on yields of secondary organic aerosol, Proc. Nat. Acad. Sci., 111, 5802-5807, doi:10.1073/pnas.1404727111, 2014.

Zotter, P., El-Haddad, I., Zhang, Y., Hayes, P. L., Zhang, X., Lin, Y.-H., Wacker, L., Schnelle-Kreis, J., Abbaszade, G., Zimmermann, R., Surratt, J. D., Weber, R., Jimenez, J. L., Szidat, S., Baltensperger, U., and Prévôt, A. S. H.: Diurnal cycle of fossil and nonfossil carbon using radiocarbon analyses during CalNex, J. Geophys. Res.-Atmos., 119, 6818-6835, doi:10.1002/2013JD021114, 2014.

Simulating Secondary Organic Aerosol in a Regional Air Quality Model Using the Statistical Oxidation Model: 2. Assessing the Influence of Vapor Wall Losses

Christopher D. Cappa[1,*], Shantanu H. Jathar[2], Michael J. Kleeman[1], Kenneth S. Docherty[3], Jose L. Jimenez[4], John H. Seinfeld[5], Anthony S. Wexler[1]

[1] Department of Civil and Environmental Engineering, University of California, Davis, CA, USA

[2] Department of Mechanical Engineering, Colorado State University, Fort Collins, CO, USA

[3] Alion Science and Technology, Research Triangle Park, NC, USA

[4] Cooperative Institute for Research in Environmental Sciences and Department Chemistry and Biochemistry, University of Colorado, Boulder, CO, USA

[5] Division of Chemistry and Chemical Engineering and Division of Engineering and Applied Science, California Institute of Technology, Pasadena, CA, USA

Correspondence to: C. D. Cappa (cdcappa@ucdavis.edu)

1   Abstract

The influence of losses of organic vapors to chamber walls during secondary organic aerosol (SOA) formation experiments has recently been established. Here, the influence of such losses on simulated ambient SOA concentrations and properties is assessed in the UCD/CIT regional air quality model using the statistical oxidation model (SOM) for SOA. The SOM was fit to laboratory chamber data both with and without accounting for vapor wall losses following the approach of Zhang et al. (2014). Two vapor wall loss scenarios are considered when fitting of SOM to chamber data to determine best-fit SOM parameters, one with "low" and one with "high" vapor wall-loss rates to approximately account for the current range of uncertainty in this process. Simulations were run using these different parameterizations (scenarios) for both the southern California/South Coast Air Basin (SoCAB) and the eastern United States (US). Accounting for vapor wall losses leads to substantial increases in the simulated SOA concentrations from VOCs in both domains, by factors of ~2-5 for the low and ~5-10 for the high scenario. The magnitude of the increase scales approximately inversely with the absolute SOA concentration of the no loss scenario. In SoCAB, the predicted SOA fraction of total OA increases from ~0.2 (no) to ~0.5 (low) and to ~0.7 (high),

32   with the high vapor wall loss simulations providing best general agreement with observations. In

33   the eastern US, the SOA fraction is large in all cases but increases further when vapor wall losses

34   are accounted for. The total OA/ΔCO ratio captures the influence of dilution on SOA

35   concentrations. The simulated OA/ΔCO in SoCAB (specifically, at Riverside, CA) is found to

36   increase substantially during the day only for the high vapor wall loss scenario, which is consistent

37   with observations and indicative of photochemical production of SOA. Simulated O:C atomic

38   ratios for both SOA and for total OA increase when vapor wall losses are accounted for, while

39   simulated H:C atomic ratios decrease. The agreement between simulations and observations of

40   both the absolute values and the diurnal profile of the O:C and H:C atomic ratios for total OA was

41   greatly improved when vapor wall-losses were accounted for. These results overall demonstrate

42   that vapor wall losses in chambers have the potential to exert a large influence on simulated

43   ambient SOA concentrations, and further suggest that accounting for such effects in models can

44   explain a number of different observations and model/measurement discrepancies.

45

Deleted: represents

Deleted: -corrected

Deleted: Similar improvements would likely not be possible solely through the inclusion of semi/intermediate volatility organic compounds in the simulations.

2   Introduction

Particulate organic matter, or organic aerosol (OA), is derived from primary emissions or from secondary chemical production in the atmosphere from the oxidation of volatile organic compounds (VOCs). OA makes up a substantial fraction of atmospheric submicron particulate matter (Zhang et al., 2007), influencing the atmospheric fate and impact of PM on regional and global scales. Gas-phase oxidation of VOCs leads to the formation of oxygenated product species that can condense onto existing particles or nucleate with other species to form new particles (e.g. Ziemann and Atkinson, 2012). Much of the understanding regarding the formation of secondary organic aerosol (SOA) via condensation has been derived from experiments conducted in laboratory chambers. In a typical experiment, a precursor VOC is added to the chamber and exposed to an oxidant (e.g OH, O_3 or NO_3). As both the precursor VOC and the oxidation products react with the oxidant, SOA is formed. The amount of SOA formed per amount of precursor reacted (i.e. the SOA mass yield) can then be quantified (e.g. Odum et al., 1996). Such SOA yield measurements form the basis of most parameterizations of SOA formation in regional air quality and global chemical-transport and climate models (Tsigaridis et al., 2014). However, too often simulated SOA concentrations underestimate observed values, especially in polluted regions, and sometimes dramatically so (Heald et al., 2005; Volkamer et al., 2006; Ensberg et al., 2013). There have been various efforts to account for model/measurement disparities including, most notably: (i) the addition of new SOA precursors in the form of so-called semi-volatile and intermediate volatility organic compounds, S/IVOCs, including treating primary organic aerosol as semi-volatile (Robinson et al., 2007); (ii) the addition of ad hoc "ageing" schemes on top of existing parameterizations of SOA from VOCs (Lane et al., 2008b; Tsimpidi et al., 2010; Dzepina et al., 2011); (iii) updating of aromatic SOA yields (Dzepina et al., 2009); and (iv) production of SOA in the aqueous phase in aerosol-water, clouds and fogs (Ervens et al., 2011). More recently, concerns over the influence of vapor wall losses on the experimental chamber data used to develop the parameterizations have arisen (Matsunaga and Ziemann, 2010; Zhang et al., 2014). The influence of erroneously low SOA yields due to vapor wall losses on simulated SOA concentrations in three-dimensional regional models and properties is the focus of the current work.

Recent observations have demonstrated that organic vapors can be lost to Teflon chamber walls, and that the extent of loss is related to the compound vapor pressures with lower vapor pressure compounds partitioning more strongly to the walls than higher vapor pressure compounds

3

82 (Matsunaga and Ziemann, 2010; Kokkola et al., 2014; Krechmer et al., 2015; Yeh and Ziemann,

83 2015; Zhang et al., 2015). These results suggest that vapor wall losses during SOA formation

84 experiments could potentially bias observed SOA concentrations. Indeed, Zhang et al. (2014)

85 observed that SOA yields from toluene + OH photooxidation depend explicitly on the seed particle

86 surface area, all other conditions being equal. They interpreted these observations using a dynamic

87 model of particle growth coupled with a parameterizable gas-phase chemical mechanism, the

88 statistical oxidation model (SOM) (Cappa and Wilson, 2012). They determined that substantial

89 vapor wall losses were most likely the cause of this dependence, with biases of up to a factor of

90 ~4 for these experiments. Further, they estimated for this system that the vapor wall loss rate

91 coefficient (k_{wall}) was ~2 x 10^{-4} s^{-1} for their 25 m^3 chamber. This value of k_{wall} is in reasonable

92 agreement both with theoretical expectations—so long as the vapor-wall accommodation

93 coefficient (α_{wall}) is >10^{-5}—and with results of Ziemann and colleagues (Matsunaga and Ziemann,

94 2010; Yeh and Ziemann, 2015) who estimated k_{wall} ~ 6 x 10^{-4} s^{-1} for their 8 m^3 chamber. Kokkola

95 et al. (2014) have also suggested vapor wall losses can impact SOA yields, although they

96 determined a much larger k_{wall} of ~10^{-2} s^{-1} for their 4 m^3 chamber. Recent direct measurements of

97 k_{wall} for a range of oxidized VOCs (OVOCs), produced from reactions of VOCs in traditional

98 chambers, suggest that k_{wall} can vary by an order of magnitude (~ 2 x 10^{-6} – 3 x 10^{-5} s^{-1}) and that

99 k_{wall} is dependent on the OVOC vapor pressure (Zhang et al., 2015); such low k_{wall} values implies

100 that the α_{wall} is < 10^{-5} and controls the rate of vapor loss to the walls.

101   Although the exact value of k_{wall} is likely chamber-specific (which likely contributes to some

102 of the above-mentioned variability in k_{wall}) and thus the exact influence of vapor wall losses on

103 chamber SOA measurements remains somewhat uncertain, the preponderance of evidence

104 suggests that such effects are important. Existing SOA parameterizations have typically not been

105 determined with explicit accounting for vapor wall losses. Consequently, they likely underestimate

106 actual SOA formation in the atmosphere where walls are much less important (although dry

107 deposition of vapors may still be a factor (Hodzic et al., 2014)). Two recent efforts have attempted

108 to estimate the influence of vapor wall losses on SOA concentrations in the atmosphere (Baker et

109 al., 2015; Hayes et al., 2015). One of the studies (Baker et al., 2015) builds on the existing two-

110 product parameterization of SOA formation in the Community Multiscale Air Quality (CMAQ)

111 model and simply scales the yields of the semi-volatile products up by factors of 4. In the two-

112 product model, a given VOC reacts to form two semi-volatile products that partition to the

4

113   condensed phase. The semi-volatile products are formed with mass yields, y_i, and partitioning
114   coefficients, K_i, that have been determined by fitting the model to data from chamber experiments
115   in which vapor wall losses were not accounted for. The other study (Hayes et al., 2015) used a
116   similar yield-scaling approach, but within the volatility basis set (VBS) four-product framework
117   to represent SOA formation, and they scaled the mass yields for only the semi-volatile product
118   species from aromatics. Not surprisingly, these simple *ad hoc* scaling methods demonstrated that
119   increasing the yields of the semi-volatile products from their originally parameterized values
120   increases the simulated SOA concentration, but quantitative interpretation of the results is difficult.
121   This is an especially important consideration given that different SOA systems may exhibit
122   different sensitivities to vapor wall losses, owing to differences in the product species volatility
123   distribution and the extent to which multi-generational ageing influences the SOA formation. More
124   robust assessment of the influence of vapor wall losses on simulated SOA concentrations in
125   regional air quality models is thus needed.

126   In this study, the SOM SOA model (Cappa and Wilson, 2012) is utilized to examine the
127   influence of vapor wall losses on simulated SOA concentrations and O:C atomic ratios in a 3D
128   regional air quality model, specifically the UCD/CIT (Kleeman and Cass, 2001). What
129   distinguishes the present approach is that the potential influence of vapor wall losses is inherently
130   accounted for during the development of the SOM SOA parameterization (Zhang et al., 2014).
131   This can be contrasted with a simple scaling of an existing parameterization. The current approach
132   allows for more detailed characterization of different precursor species, reaction conditions (e.g.
133   NO_x sensitivities) and the complex interplay of various timescales (reaction, gas/wall partitioning
134   and gas/particle partitioning). This also allows for examination of the extent to which different
135   assumptions regarding the value of k_{wall} (i.e. the first-order rate constant for vapor loss to chamber
136   walls) during development of the SOA parameterization impact simulations of ambient SOA
137   concentrations. Further, the SOM framework simulates O:C atomic ratios in addition to OA mass
138   concentrations, and thus allows for more detailed assessment of the simulated OA and comparison
139   with observations. Our results demonstrate that accounting for vapor wall losses can have a
140   substantial impact on simulated SOA concentrations and suggest that there may be regionally-
141   specific differences.

142

5

3 Methods

3.1 Air quality model

Regional air quality simulations were performed using the UCD/CIT chemical transport model (Kleeman and Cass, 2001) for two geographical domains: (i) the Southern California Air Basin (SoCAB) and (ii) the eastern US. Details regarding the general model configuration and emissions inventory used have been previously discussed (Jathar et al., 2015a), and the reader is referred to that work for further information. Details specific to the current work are provided in the following sections. Model simulations were run for SoCAB from July 20 to August 2, 2005 and for the eastern US from August 20 to September 2, 2006. Model spatial resolution was higher in SoCAB (8 km x 8 km) than in the eastern US (36 km x 36 km) to account for the different domain sizes.

3.2 Statistical Oxidation Model for SOA

SOA formation from six VOC classes was simulated using the statistical oxidation model (Cappa and Wilson, 2012; Cappa et al., 2013), which was recently implemented in the UCD/CIT model (Jathar et al., 2015a). The VOC classes considered are: long alkanes, benzene, high-yield aromatics (i.e. toluene), low-yield aromatics (i.e. m-xylene), isoprene and terpenes (including both mono- and sesquiterpenes). SOM is a parameterizable model that simulates the multi-generational oxidation of the product species formed from reaction of the SOA precursor VOCs. In SOM, a "species" is defined as a molecule with a specific number of carbon and oxygen atoms (N_C and N_O, respectively), and where the VOC-specific properties of these SOM species are determined through fitting to laboratory observations. Reactions of a SOM species lead to either functionalization (i.e. addition of oxygen atoms while conserving the number of carbon atoms) or fragmentation (i.e. the production of two species which individually have fewer carbon atoms but where the total carbon is conserved, and where each new species adds one additional oxygen atom). The particular tunable parameters in SOM are: the probability of adding one, two, three or four oxygen atoms per reaction, referred to as p_{XO}; the decrease in vapor pressure per added oxygen, referred to as ΔLVP; and the probability of fragmentation, which is related to the O:C atomic ratio of a given species as $P_{frag} = (O:C)^{m_{frag}}$ and where m_{frag} is the tunable parameter. SOA formation from the semi-volatile SOM species assumes that partitioning is described according to absorptive gas-particle partitioning theory (Pankow, 1994), and the gas-particle mass

6

172 transfer has been simulated using dynamic partitioning (Kleeman and Cass, 2001; Zhang et al.,
173 2014; Jathar et al., 2015a). The parameters used in the current work have been determined by
174 fitting to time-dependent data from SOA formation experiments conducted in the Caltech chamber
175 both with and without accounting for vapor wall losses during the fitting process (discussed further
176 below); references for the specific experiments considered are provided in Table S1. The specific
177 influence of considering multi-generational ageing on simulated SOA concentrations and
178 properties is discussed in a companion paper (Jathar et al., 2015b). The use of the SOM to represent
179 SOA formation leads to an increase of about a factor of 2.5 or less in computer processing time
180 required compared to use of the 2-product model.

181 **3.3 Accounting for Vapor Wall Loss**

182 3.3.1 SOM

183 Vapor wall losses have been accounted for using SOM, as detailed in Zhang et al. (2014).
184 Vapor wall loss is treated as a reversible, absorptive process with vapor uptake specified using a
185 first-order rate coefficient (k_{wall}) and the desorption rate related to the effective saturation
186 concentration, C^*, of the organic species and the effective absorbing mass of the walls (Matsunaga
187 and Ziemann, 2010). Unique SOM fits (i.e. values of m_{frag}, ΔLVP and p_{XO}) have been determined
188 for different assumed values of k_{wall}. Best-fit values are provided in Table S1. It should be noted
189 that the influence of vapor wall losses is inherent in the fit parameters, and in the absence of walls
190 (i.e. in the atmosphere) the predicted SOA formed will be larger when the fits account for vapor
191 wall losses. A base case set of parameters with no vapor wall losses assumed during fitting (termed
192 SOM-no) was determined using $k_{wall} = 0$. In Zhang et al. (2014), an optimal value of $k_{wall} = 2$ x 10^-
193 ^{4} s^{-1} was determined for the California Institute of Technology chamber based on simultaneous
194 fitting of the SOM to a set of toluene photooxidation experiments conducted at different seed
195 particle concentrations. Unlike in Zhang et al. (2014), the values of k_{wall} used here were not
196 determined during model fitting. This is because the absolute value of k_{wall} is not well constrained
197 by a single experiment, and the simulations require vapor wall loss corrected parameters for VOCs
198 besides toluene. Therefore, two specific bounding cases that account for vapor wall loss are instead
199 considered based on the results from Zhang et al. (2014). Specifically, values of $k_{wall} = 1$ x 10^{-4} s^{-1}

Deleted: Here,

Deleted: = 0,

202 and 2.5 x 10^{-4} s^{-1} are considered, corresponding to a low vapor wall loss case (SOM-low) and high
203 vapor wall loss case (SOM-high), respectively.

204   An important aspect of vapor wall loss is that the impact it has on SOA concentrations is
205 dependent upon the timescale associated with vapor-particle equilibration (τ_{v-p}) (McVay et al.,
206 2014; Zhang et al., 2014). The τ_{v-p} is related to the accommodation coefficient associated with
207 vapor condensation on particles, $\alpha_{particle}$. Above a vapor-particle accommodation coefficient of
208 $\alpha_{particle} \sim 0.1$ variations in the exact value of $\alpha_{particle}$ does not influence the effects of vapor wall
209 losses. This is not to say that vapor wall losses have no influence on the amount of SOA formed
210 when $\alpha_{particle} \geq 0.1$, only that the net impact does not depend on $\alpha_{particle}$. Below this value, vapor-
211 particle equilibrium is slowed and the effects of loss of vapors to the walls are accentuated. Thus,
212 a conservative estimate that minimizes the influence of vapor wall losses on SOA formation is

213 obtained using $\alpha_{particle} \geq 0.1$. Here, data fitting and parameter determination was performed
214 assuming that $\alpha_{particle} = 1$, and is thus a conservative estimate.

215   SOM was fit to time-dependent SOA formation experiments conducted in the California
216 Institute of Technology chamber, following the methodologies described in Cappa et al. (2013)
217 and Zhang et al. (2014). Observed suspended particle concentrations have been corrected only for
218 physical deposition on chamber walls, which is appropriate since vapor wall losses are accounted
219 for separately by SOM. Best-fit values for the SOM parameters for the base case (SOM-no) are
220 given in Jathar et al. (2015a) and values for SOM-low and SOM-high determined here are given
221 in Table S1, along with the sources of the experimental data. Parameters have been separately
222 determined for experiments conducted under low-NO$_x$ and high-NO$_x$ conditions since the SOA
223 yields differ. Example results that illustrate the influence of vapor wall losses on simulated SOA
224 yields are presented in Figure S1 for box model simulations that have been conducted using the
225 best-fit parameters determined for toluene SOA (low-NO$_x$ conditions), but where the simulations
226 are run assuming there are no walls (i.e. by setting $k_{wall} = 0$).

227 ### 3.3.2 Two-product model

228   Ideally, SOA levels from the SOM-based simulations can be compared with similar results
229 based on the commonly used two-product model. To do so involves determining new parameters
230 for the two-product model in which vapor wall losses are explicitly accounted for. Therefore, vapor

8

237 wall-loss corrected SOA yield curves (i.e. [SOA] versus [ΔHC], where ΔHC is the concentration

238 of reacted hydrocarbon) were generated with SOM using the parameters determined by fitting

239 SOM to the original chamber data when $k_{wall} > 0$, but now where k_{wall} is set to zero. The 2-product

240 model could then be fit to these "corrected" yield curves to determine vapor wall-loss corrected

241 yields and partitioning coefficients. These new fits would inherently account for the influence of

242 vapor wall loss since the two-product model is being fit to the corrected "wall-less" data and thus

243 differ from *ad hoc* scaling of yields. However, it was determined that the two-product fits were

244 not sufficiently robust across the entire suite of compounds and vapor wall loss conditions

245 considered to be implemented in the atmospheric model. An example for SOA from dodecane +

246 OH under low-NO$_x$ reaction conditions is shown in Figure S2. We have determined that this lack

247 of robustness is a result of the limited dynamic range of the 2-product model. This can be

248 contrasted with the SOM, which includes many more species that span a wider, more continuous

249 volatility range, making it more flexible when fitting the laboratory data. More specifically, the

250 SOA concentrations from the chamber observations, both uncorrected and corrected, ranged from

251 ~1-500 μg m^{-3}, often with few data points at concentrations less than ~10 μg m^{-3}. Thus, when fits

252 were performed, inconsistent behavior between the different vapor wall loss conditions was

253 obtained over the atmospherically relevant concentration range (~0.1-20 μg m^{-3}). Attempts were

254 made to fit the two-product model over a restricted concentration range or to fit using log([SOA])

255 instead of [SOA]. However, neither effort led to sufficiently robust results (although both did lead

256 to improvements). This null result suggests that simple scaling of two-product yields (Baker et al.,

257 2015) to account for the effects of vapor wall losses may not be appropriate. This may similarly

258 apply to scaling of VBS parameters (Hayes et al., 2015), although the greater flexibility of the

259 VBS (commonly implemented with four products, instead of two) can potentially allow for unique

260 "wall-less" fits to be determined (Hodzic et al., Submitted). The extent to which such alternative

261 methods can robustly account for vapor wall losses that are computationally less intensive than

262 SOM will be explored in future work.

3.4 Primary Organic Aerosol and IVOCs

264 Primary organic aerosol (POA) derived from anthropogenic (e.g. vehicular activities, food

265 cooking) or pyrogenic (e.g. wood combustion) sources are simulated assuming that the POA is

266 non-volatile. This is the standard assumption in the CMAQ model framework (Simon and Bhave,

9

267 2011), and thus is adopted here. It is known that some POA is semi-volatile, not non-volatile as
268 assumed here. Had POA been treated within a semi-volatile framework (Robinson et al., 2007),
269 such that some fraction of the POA can evaporate (i.e. SVOCs) and react within the gas-phase and
270 be converted to SOA (sometimes improperly referred to as "oxidized POA"), then the amount of
271 POA would likely decrease (due to evaporation) and the amount of simulated SOA would increase
272 (due to condensation of oxidized SVOC vapors); the total OA concentration (POA + SOA) may
273 or may not increase as a result, depending on the details of the parameterization and the
274 atmospheric conditions. Additionally, nearly all modeling efforts in which POA is treated as semi-
275 volatile have also included contributions from gas-phase IVOCs as an added class of SOA
276 precursors; these two issues are rarely implemented independently in models, although their
277 contributions can be separately tracked. Whereas simply treating POA as semi-volatile may or
278 may not lead to an increase in the total OA concentration, the introduction of new SOA precursor
279 mass in the form of IVOCs will inevitably lead to production of more SOA in the model. The
280 relative importance of IVOCs will depend on the amount of added IVOC mass and the propensity
281 of these IVOC vapors to form SOA in the model (i.e. their effective SOA yield). In the current
282 study, we do not explicitly consider the potential for IVOCs to contribute to the ambient SOA
283 burden, focusing instead on how vapor wall losses influence SOA formation from VOCs. We will
284 aim to consider contributions from IVOCs and how they are influenced by vapor wall losses in
285 future studies. Regardless, the implications of our particular treatment (non-volatile POA
286 excluding IVOCs) are discussed below.

3.5 Model Simulations and Outputs

288   Six individual model simulations have been carried out to determine the spatial distribution of
289 SOA concentrations. Each simulation used one of the SOM parameterizations, i.e. SOM-no, SOM-
290 low or SOM-high with either the low- and high-NO_x parameters. Each precursor VOC is allowed
291 to react with either OH, O_3 or NO_3 as characterized by an oxidant-specific rate coefficient,
292 although the products and product distributions of the first-generation products are assumed to be
293 oxidant independent. This simplification is identical to that employed in CMAQv4.7 (Carlton et
294 al., 2010). Reactions of subsequent oxidized SOM products then occur only via reaction with OH
295 radicals according to the SOM parameterization associated with that precursor VOC (as
296 determined by fitting the photooxidation experiments). Besides the absolute SOA concentration,

10

297   SOM also allows for explicit calculation of the average (and precursor-specific) O:C and H:C

298   atomic ratios and of the SOA volatility distribution, which characterizes the distribution of

299   particulate and gas-phase mass concentrations with respect to C^*. To estimate the O:C of the total

300   OA (POA + SOA), it is assumed that the non-volatile POA has a constant O:C = 0.2 and H:C =

301   2.0 (Ng et al., 2011). Since the simulated $(O:C)_{total}$ is just a combination of $(O:C)_{SOA}$ and $(O:C)_{POA}$,

302   assuming a different value for $(O:C)_{POA}$ would change the absolute value of $(O:C)_{total}$ but not any

303   dependence on simulation conditions. This is similarly true for $(H:C)_{total}$.

304   As noted above, unique sets of SOM parameters were fit to experiments conducted under either

305   low- or high-NO_x conditions assuming a particular value for k_{wall}. Since each simulation used a

306   single set of SOM fit parameters (e.g. SOM-no fit to low-NO_x experiments) the SOA NO_x

307   parameterization used in a given simulation is independent of the actual simulated ambient NO_x

308   concentrations or NO/HO_2 ratio. Consequently, comparison between the simulations conducted

309   using the low- and high-NO_x parameterizations gives an indication of the range expected from

310   variability in NO_x levels, and the average between the two simulations provides a representation

311   that is intermediate between these two extremes. Unless otherwise specified, reported values are

312   for the average of the simulations run using the low- and high-NO_x parameterizations. This

313   approach towards understanding the influence of NO_x is different than some previous approaches

314   that attempted to account for the SOA NO_x dependence in a more continuously variable manner.

315   For example, some simulations using the two-product approach have used the instantaneous

316   NO/HO_2 ratios predicted by the model to allow distinguishing between low- and high-NO_x

317   products and SOA yields for aromatic VOCs (Carlton et al., 2010). Similarly, instantaneous

318   VOC/NO_x ratios have been used with VBS-type models for aromatic VOCs to allow for

319   interpolation between the two regimes (Lane et al., 2008a). Typically, these efforts have not

320   considered the NO_x-dependence of monoterpene and sesquiterpene yields even though it is

321   experimentally established that the NO_x condition (and more specifically, the NO/HO_2 ratio)

322   influences SOA yields for both aromatic and biogenic compounds (e.g. Ng et al., 2007a; Ng et al.,

323   2007b). For most VOCs, the functional dependence of the SOA yield on the VOC/NO_x ratio or the

324   NO/HO_2 ratio is not well established, making it difficult to understand how well the interpolation

325   methods work. (SOA formation from isoprene is a notable exception (e.g. Xu et al., 2014).)

326   Further, modeled NO/HO_2 ratios may be off by orders of magnitude, most likely due to poor

327   representation of HO_2 concentrations (Carlton et al., 2010), making it difficult to understand how

11

328 well the conditions of the laboratory translate to the model environment. By considering the low-

329 and high-NO_x parameterizations separately, i.e. the approach used in the current study, bounds on

330 the overall influence of NO_x on the simulated SOA can be established. However, this approach

331 will not capture how the simulated SOA may vary due to spatial and temporal variations in the

332 model NO_x and oxidant fields. Future efforts will aim to account for the NO_x-dependence of SOA

333 formation in a more continuously varying manner, and to account for recent updates to the detailed

334 isoprene oxidation mechanism (Pye et al., 2013).

335 **4   Results and Discussion**

336 **4.1   General influence of vapor wall loss on simulated SOA**

337   The spatial distribution of the SOM-no model SOA concentrations is shown for SoCAB and

338 the eastern US using the average from the simulations carried out using the low- and high-NO_x

339 parameterizations (Figure 1a-b). (Again, the low- and high-NO_x designations here refer only to the

340 experimental conditions under which the SOM parameters were determined, not the actual NO_x

341 conditions in the UCD/CIT model.) For SoCAB, predicted SOA concentrations are largest in and

342 around downtown Los Angeles and in the forested regions of the Los Padres National Forest and

343 the Santa Monica Mountains National Recreation Area in the NW quadrant. The spatial

344 distribution of SOA is similar to that obtained using the conventional two-product SOA

345 parameterization (Jathar et al., 2015a, b). For the eastern US, predicted SOA concentrations are

346 largest in the southeast, in particular around Atlanta, Georgia. Overall, the simulated SOA

347 concentrations with the SOM-no model are larger in the eastern US than in SoCAB, reflecting the

348 relatively strong influence of biogenic emissions in this region.

349   The influence of vapor wall losses on the simulated ambient SOA concentrations is illustrated

350 in Figure 1c-f as the ratio between the SOA from the SOM-low and SOM-high simulations to the

351 SOM-no (no wall losses) simulation. This ratio will be referred to generally as the wall loss impact

352 ($R_{wall,low}$ or $R_{wall,high}$). Values of R_{wall} larger than one indicate that accounting for vapor wall losses

353 as part of the SOM parameterization leads to an increase in the predicted SOA concentrations. In

354 the SoCAB, the $R_{wall,low}$ varies from 1.5-4.5, while the $R_{wall,high}$ varies from 3 to more than 10. The

355 largest ratios (indicating the largest impact of accounting for vapor wall losses) tend to occur in

356 more remote locations as this is where concentrations are lower (Figure 2). However, the impact

12

357 is still large in downtown Los Angeles and the greater LA region (average $R_{wall,low}$ ~2.5 and $R_{wall,high}$
358 ~5). In the eastern US, the simulated R_{wall} vary over a similar range as in SoCAB, with $R_{wall,low}$
359 varying from 1.5-5 and $R_{wall,high}$ from 3 to 10. There is again a general, although not exact, inverse
360 relationship between R_{wall} and the absolute SOA concentrations; the greater scatter in the eastern
361 US compared to SoCAB at low SOA concentrations likely reflects the larger spatial range
362 considered. The smallest simulated R_{wall} values occur across the southeast and up the eastern
363 seaboard ($R_{wall,low}$ ~2.5 and $R_{wall,high}$ ~5) while the largest values occur over the Great Lakes and
364 Michigan, Nebraska, and the Gulf of Mexico and Atlantic Ocean; there is a steep increase going
365 from land to sea. If R_{wall} values are calculated using the simulated SOA concentrations from either
366 the low-NO$_x$ or high-NO$_x$ parameterizations individually, as opposed to the average values used
367 above, very similar results are obtained (Figure SX).

368 Regional air quality models have historically overestimated the urban-to-regional gradient in
369 total OA concentrations. Robinson et al. (2007) showed that the simulated urban-to-regional
370 gradient could be reduced and made more consistent with observations by treating POA as semi-
371 volatile and adding SVOCs and IVOCs as SOA-forming species. The current results suggest a
372 complementary explanation, namely that the urban-to-regional gradient can be reduced when
373 vapor wall losses are accounted for since R_{wall} generally increases with decreasing SOA
374 concentration and since POA is identical between the different model parameterizations.
375 Consequently, larger R_{wall} are found outside of the major source regions, which decreases the
376 urban-to-regional contrast. Indeed, the ratio between the predicted average SOA in downtown LA
377 (urban) to that over the Pacific Ocean near the coast of LA (regional) and decreases from 2.3
378 (SOM-no) to 1.5 (SOM-low) to 1.3 (SOM-high), for example. Additionally, it has been suggested
379 that the typical underprediction of SOA by air quality and chemical transport models relative to
380 observations might increase with photochemical age (Volkamer et al., 2006). The current results
381 suggest the possibility that the SOA concentrations in more remote (lower concentration) regions
382 may be underestimated in models to a greater extent in a relative sense than in high-source (higher
383 concentration) regions due to a lack of accounting for vapor wall losses, although the absolute
384 differences in SOA concentrations may be larger in regions where absolute concentrations are
385 larger.

Deleted: decreases

Deleted: downtown LA (urban)

Deleted: .

13

4.2 OA composition and concentrations

The simulated fraction of total OA that is SOA (f_{SOA}) is substantially smaller in SoCAB than in the eastern US, especially the southeast US (Figure 3). The predicted f_{SOA} values vary spatially within a given region, with the SOM-no simulations in the general range of ~0.1-0.3 for SoCAB and ~0.4-0.9 for the eastern US. This difference between regions results from the substantial POA emissions in SoCAB and the large emissions of biogenic VOCs across the southeast US. Consequently, accounting for vapor wall losses has a larger impact on the absolute total OA (SOA + POA) concentrations in the eastern US than it does in SoCAB, although the impact in both regions is substantial. For SoCAB, the predicted 24-h average f_{SOA} range increases to ~0.2-0.5 for SOM-low and to ~0.4-0.8 for SOM-high simulations. These model results can be compared with measurements from the 2005 SOAR field study in Riverside, CA, which overlaps with the simulation period. The observed f_{SOA} during SOAR ranged from ~0.6 in early morning to ~0.9 in midday, with a campaign-average of ~0.78 (Docherty et al., 2011). Measurements at Pasadena, CA during a later time period, June 2010 during the CalNex study, give similar results with the campaign-average $f_{SOA} = 0.6$ (Hayes et al., 2013). (Note that here we are equating SOA with the "oxygenated organic aerosol," or OOA factors that are obtained from positive matrix factorization of the measured OA time series, and equating POA with the sum of hydrocarbon-like OA (HOA), cooking-derived OA (COA), and "local" OA (LOA).) The SOM-high simulations in SoCAB are most consistent with these observations.

For the eastern US, the predicted f_{SOA} range increases from 0.4-0.9 for SOM-no to ~0.7-0.9 for SOM-low and to ~0.8-1 for SOM-high. These predicted values can be compared with measurements made at a few locations in the southeastern US (specifically, sites in Alabama and Georgia), which show that the f_{SOA} in this region exhibits a strong seasonal dependence and some spatial variation (Xu et al., 2015b). The measurements in spring and summer indicate that the total OA is dominated by SOA, with f_{SOA} measurements ranging from 0.7 to 1 and with the smaller values observed at the more urban sites. The predicted f_{SOA} from the SOM-low and SOM-high simulations are most consistent with this range, with the f_{SOA} from the SOM-no simulations being on the low side, especially in comparison with the more rural sites.

The simulated total OA concentrations are compared to ambient OA measurements made at the STN (Speciated Trends Network) and IMPROVE (Interagency Monitoring of Protected Visual

14

419　Environments) (The Visibility Information Exchange Web System (VIEWS 2.0), 2015) air quality

420　monitoring sites in SoCAB and the eastern US; the regional differences in f_{SOA} should be kept in

421　mind for this model/measurement comparison. A map of sites is shown in Figure S3. STN sites

422　tend to be more urban and have higher OA concentrations compared to IMPROVE sites, which

423　tend to be more remote. OA concentrations are estimated as the measured organic carbon (OC)

424　concentrations times 2.1 for IMPROVE sites and as $1.6 \times$ ([OC] - 0.5 μg m^{-3}) for STN sites (Turpin

425　and Lim, 2001). The -0.5 μg m^{-3} offset for the STN sites arises because the IMPROVE data are

426　both artifact and blank corrected while the STN data are only artifact corrected (Subramanian et

427　al., 2004). The difference in scaling factors (2.1 versus 1.6) approximately accounts for differences

428　in the OA/OC conversion between more urban and more rural networks (Turpin and Lim, 2001).

429　Given the generally regional character of OA in much of the eastern US, it may be that the

430　difference in OM/OC between the STN and IMPROVE sites may be smaller than assumed here

431　(most likely with the 1.6 being too low, leading potentially to an underestimate in the OA at the

432　STN sites). We note that IMPROVE data may also be biased low by ~25% in the SE US summer

433　due to evaporation after sampling (Kim et al., 2015).

434　　　Table 1 lists statistical metrics of fractional bias, normalized mean square error (NMSE) and

435　the concordance correlation coefficients that capture model performance for OA for all simulations

436　for both domains across the STN and IMPROVE monitoring networks. Fractional bias is

437　calculated as:

438　$Fractional\ bias = \dfrac{2(c_{OA,sim} - c_{OA,obs})}{c_{OA,sim} + c_{OA,obs}}$　　　　　　　　　　(1)

439　and the NMSE as

440　$NMSE = \left| \dfrac{(c_{OA,sim} - c_{OA,obs})^2}{c_{OA,sim} \times c_{OA,obs}} \right|$　　　　　　　　　　(2)

441　where the subscripts *sim* and *obs* refer to the simulated and observed OA concentrations,

442　respectively. The concordance correlation coefficients (ρ_c) are calculated as:

443　$\rho_c = \dfrac{2s_{sim,obs}}{s_{sim}^2 + s_{obs}^2 + (\overline{C_{OA,sim}} - \overline{C_{OA,obs}})^2}$　　　　　　　　　　(3)

444　where $\overline{C_{OA,sim}}$ and $\overline{C_{OA,obs}}$ indicate the mean, s_{sim}^2 and s_{obs}^2 are the variance and $s_{sim,obs}$ is the

445　covariance of the simulated and observed OA concentrations. Scatter plots are shown in Figure S4

15

Deleted: and

447   and Figure S5; many more sites are considered in the eastern US than in the SoCAB given the
448   larger geographical domain and distribution of sites. In both regions, the SOM-no simulations
449   underpredict the STN and IMPROVE observations, especially in the SoCAB. The negative bias
450   of the SOM-no simulations is generally improved as vapor wall losses are accounted for. For both
451   the STN and IMPROVE sites in the SoCAB the SOM-high simulations give best agreement. For
452   the eastern US STN sites, an average of the SOM-low and SOM-high simulations provides the
453   best agreement. For the eastern US IMPROVE sites, the SOM-low simulations provide the best
454   agreement, although with some overprediction. (If the eastern US STN and IMPROVE
455   measurements do underestimate the actual OA concentrations, the degree to which accounting for
456   vapor wall losses improves the model-measurement comparison will increase.) The simulated
457   anthropogenic/biogenic SOA split is found to be approximately the same at sites within both
458   networks (e.g. Figure 4). This occurs even though the IMPROVE sites tend to be more remote
459   than the STN sites in the eastern US, and reflects the regional character of SOA in that region.
460   Ultimately, the comparisons suggest that accounting for vapor wall losses can improve model-
461   measurement agreement, although there are differences in terms of whether the SOM-high
462   simulations or SOM-low simulations produce the best agreement. That the OA concentrations for
463   the SOM-high simulations remains slightly lower than the observations for STN sites in SoCAB
464   could potentially result from the non-volatile treatment of POA, the exclusion of IVOCs in the
465   current model or uncertainty in the POA emission inventory.

466   The simulations can also be compared with observations of the OA-to-ΔCO concentration ratio
467   (OA/ΔCO) during SOAR (Docherty et al., 2008; Docherty et al., 2011), and where ΔCO indicates
468   the background corrected CO concentration. Because CO is relatively long lived, normalization of
469   the calculated and observed OA to the concurrent background-corrected CO helps to minimize the
470   impacts of uncertainties in boundary layer dynamics and accounts for variability in emissions and
471   transport to some extent (De Gouw and Jimenez, 2009). The background-corrected CO
472   concentration is calculated as $\Delta[CO] = [CO] - [CO]_{bgd}$. The estimated $[CO]_{bgd}$ for the observations
473   is 105 ppb (with a plausible range from 85-125 ppb) (Hayes et al., 2013). In contrast, the $[CO]_{bgd}$
474   for the model is estimated to be 130 ppb based on the simulated [CO] over the open ocean west of
475   Los Angeles. The observed diurnal profile of OA/ΔCO during SOAR exhibits a distinct peak
476   around mid-day, corresponding to the peak in photochemical activity. This indicates a substantial
477   influence of SOA production on the total OA concentration (Figure 5) (Docherty et al., 2008). The

16

478   simulated OA/ΔCO diurnal profiles around Riverside for the SOM-high simulations are most
479   consistent with the observations, exhibiting a distinct peak around mid-day that is similar to the
480   observations (Figure 5). Unlike the observations, the diurnal OA/ΔCO profile for the SOM-no
481   simulation exhibits almost no increase during mid-day and the SOM-low simulation exhibits only
482   a slightly larger daytime increase. The slope of a one-sided linear fit to a graph of the observed
483   [OA] versus [CO] during daytime (10 am to 8 pm) is 69 ± 2 μg m^{-3} ppm^{-1} (Figure 5) when
484   constrained to go through the assumed [CO]$_{bgd}$. This can be compared with the simulation results,
485   which have constrained slopes of 23.0 ± 0.4, 34.0 ± 0.8 and 55 ± 2 μg m^{-3} ppm^{-1} for SOM-no,
486   SOM-low and SOM-high, respectively (Figure 5g-i). Clearly the SOM-high simulations are in best
487   overall agreement with the SOAR observations. However, the maximum in the simulated OA/ΔCO
488   peaks at a smaller value than was observed. The simulated peak also occurs slightly earlier than
489   the maximum in the observations, which could be due to discrepancies in the transport to the
490   Riverside site or to too fast SOA formation in the model. Nonetheless, these results clearly indicate
491   that accounting for vapor wall losses has the potential to reconcile simulated SOA diurnal behavior
492   with observations. Alternatively or complementarily, daytime increases in the OA/ΔCO ratio from
493   SOA production can be achieved with the introduction of additional SOA precursor material such
494   as S/IVOCs (Zhao et al., 2014; Hayes et al., 2015), which are not considered here. The addition of
495   S/IVOCs would increase the daytime OA/ΔCO for all of the simulations. The magnitude of the
496   increase would depend on the amount of added S/IVOCs and the properties assigned to the
497   S/IVOCs regarding their SOA formation timescale and yield. Consideration of SOA from
498   S/IVOCs in the SoCAB using the SOM framework will be the subject of future work.

499   **4.3   SOA Composition**

500   4.3.1 Source/VOC Precursor Dependence

501   Accounting for vapor wall losses leads to regionally-specific changes in the simulated
502   contributions from the different VOC classes (e.g. TRP1, ARO1) to the SOA burden, as illustrated
503   in Figure 4 for two sites in SoCAB (central Los Angeles and Riverside) and two in the eastern US
504   (Atlanta and the Smoky Mountains). Focusing first on contributions from the biogenic VOCs, at
505   all locations accounting for vapor wall losses leads to an increase in the fractional contribution of
506   isoprene SOA, typically at the expense of terpene and sesquiterpene SOA. This is true for both the

17

507 low- and high-NO$_x$ simulations. Recent observations suggest that isoprene SOA produced via the
508 low-NO IEPOX (isoprene epoxydiol) pathway can be uniquely identified from analysis of aerosol
509 mass spectrometer measurements when the relative contribution is sufficiently large (> ~5%) (e.g.
510 Budisulistiorini et al., 2013; Hu et al., 2015). This observed IEPOX SOA accounts for around 30%
511 (May) and 40% (August) of total SOA or around 20% (May) and 30% (August) of total OA in
512 Atlanta in the summer (Xu et al., 2015a), albeit not during the same time period as simulated here.
513 IEPOX SOA was also found to account for 17% of total OA at a rural site in Alabama in 2013 (Hu
514 et al., 2015). The SOM-low and SOM-high simulation results for Atlanta are most consistent with
515 the observations, with a predicted isoprene SOA fraction of 27% and 35%, respectively, compared
516 to only 17% for the SOM-no simulations and where the reported values are for the simulations that
517 use the low-NO$_x$ parameterizations since this is the pathway that leads to IEPOX SOA. The related
518 isoprene OA fractions are 10%, 21% and 31% for the SOM-no, -low and -high simulations,
519 respectively. (These isoprene SOA fractions change only marginally for SOM-low and SOM-high
520 simulations when the high-NO$_x$ parameterizations are used, to 25% and 37%, respectively. The
521 SOM-no simulations exhibit somewhat greater sensitivity to the NO$_x$ parameterization, with the
522 high-NO$_x$ parameterization giving an SOA fraction of 7%.)

523   In SoCAB, the predicted average isoprene SOA fraction in central LA is relatively large for
524 the SOM-low (36%) and SOM-high (47%) simulations, compared to the SOM-no simulations
525 (12%). There is a large difference in SoCAB between the simulations that use the low-NO$_x$ and
526 high-NO$_x$ parameterizations, with the isoprene SOA fractions being much larger with the high-
527 NO$_x$ parameterizations (e.g. 58% for high-NO$_x$ versus 36% for low-NO$_x$ for the SOM-high
528 simulations). Measurements at Pasadena during the 2010 CalNex study did not distinctly identify
529 IEPOX SOA, which is interpreted as the IEPOX SOA contribution being lower than ~5% of the
530 OA (Hu et al., 2015). It is possible that additional isoprene SOA had been formed under higher
531 NOx conditions (compared to the southeast US) such that it is chemically different from IEPOX-
532 SOA and was not identified as a uniquely isoprene-derived SOA component, instead contributing
533 generically to the overall oxygenated OA pool. The concentration of isoprene SOA from specific
534 high-NO$_x$ pathways may, however, be limited at higher temperatures, such as found in
535 summertime Pasadena, due to thermal decomposition of intermediate gas-phase species (Worton
536 et al., 2013), although it is not clear to what extent this influenced the CalNex observations or
537 would have affected the model results had it been explicitly considered. Additionally, it should be

18

538 kept in mind that the ambient NO_x concentrations in SoCAB have decreased substantially from
539 2005-2013 (Russell et al., 2012). Thus, although the CalNex measurements do not provide direct
540 support for such a large isoprene SOA fraction, they also do not rule it out.

541   While the predicted isoprene SOA fraction increased, the predicted terpene and sesquiterpene
542 SOA fractions decreased in the simulations that accounted for vapor wall losses. Additionally, the
543 terpene SOA/sesquiterpene SOA ratio increased at all locations for the SOM-low and SOM-high
544 simulations, in large part because the sesquiterpene yield is already large and thus accounting for
545 vapor wall losses has a limited influence on the simulated sesquiterpene SOA concentrations.

546   There are some changes in the anthropogenic fraction of SOA when vapor wall losses are
547 accounted for. The anthropogenic fraction of SOA is defined here as the sum of the SOA from
548 long alkanes and aromatics, which are emitted from combustion of fossil fuels, divided by the sum
549 of the total SOA, which additionally includes SOA from isoprene, monoterpenes and
550 sesquiterpenes emitted by trees, plants and other natural sources. The ^{14}C isotopic signature of
551 fossil-derived VOCs is different from that of biogenically derived VOCs, and thus their respective
552 contributions to SOA can be partially constrained via experimental analysis of the ^{14}C content of
553 OA (Zotter et al., 2014). We assume the anthropogenic fraction is equivalent to the fossil fraction
554 of SOA (termed $F_{SOA,fossil}$). At the two eastern US sites (Atlanta and Smokey Mountains) the
555 average $F_{SOA,fossil}$ increases slightly from 14% (SOM-no) to 22% (SOM-low) and 25% (SOM-
556 high). At the two SoCAB sites (downtown LA and Riverside) the predicted average $F_{SOA,fossil}$
557 decreases slightly, from 35% (SOM-no) to 29% (SOM-low) and 30% (SOM-high), respectively.
558 In SoCAB the $F_{SOA,fossil}$ values differ between the low- and high-NO_x parameterizations, with
559 $F_{SOA,fossil}$ typically larger for the low-NO_x parameterizations (e.g. 35% for low-NO_x and 25% for
560 high-NO_x). In the eastern US, the predicted $F_{SOA,fossil}$ exhibit a stronger response to vapor wall
561 losses for the high-NO_x parameterization than the low-NO_x parameterization, although the
562 absolute values are reasonably similar. Of the anthropogenic SOA (aromatics + alkanes), the high-
563 NO_x parameterizations indicate an increasing alkane SOA fraction as vapor wall losses are
564 accounted for in both regions. In contrast, the low-NO_x parameterizations indicate minor
565 contributions from alkane SOA for all of the simulations. In general, chamber SOA yields from
566 aromatic compounds are larger for low-NO_x conditions (Ng et al., 2007a), which could help to
567 explain these differences.

19

Deleted: (here, the sum of long alkanes and aromatics) when vapor wall losses are accounted for.

570 The SoCAB $F_{\text{SOA,fossil}}$ values can be compared with estimates of the fossil fraction of "oxidized
571 organic carbon" ($F_{\text{OOC,fossil}}$) from measurements made during CalNex in Pasadena (Zotter et al.,
572 2014). It should be noted that while $F_{\text{SOA,fossil}}$ includes contributions from both oxygen and carbon
573 mass the $F_{\text{OOC,fossil}}$ includes only the carbon mass. The fossil fraction of secondary organic carbon
574 (SOC) can be calculated from the simulated SOA concentrations by accounting for the differences
575 in the O:C atomic ratios of the different SOA types to facilitate more direct comparison between
576 the simulations and observations. Specifically, the SOC mass concentration (C_{SOC}) is related to the
577 SOA mass concentration (C_{SOA}) for a given SOA type through the relationship:

$$C_{SOC} = C_{SOA} \cdot \frac{N_C \cdot MW_C}{MW_{SOA}} = \frac{N_C \cdot MW_C}{N_C \cdot MW_C + N_O \cdot MW_O + N_H \cdot MW_H} = \frac{C_{SOA}}{\frac{4}{3}(O{:}C) + \frac{1}{12}(H{:}C) + 1} \qquad (4)$$

579 where MW_C, MW_O, MW_H are the molecular weights of carbon, oxygen and hydrogen atoms,
580 respectively. The O:C and H:C values of the different SOA types are not constant in the SOM due
581 to the continuous evolution of the product distribution. However, for a given SOA type the
582 simulated O:C and H:C values vary over a relatively narrow range (Cappa et al., 2013) and thus
583 an average value can be used. The resulting $F_{\text{SOC,fossil}}$ values are compared with the $F_{\text{SOA,fossil}}$ values
584 in Table S2 and are found to be very similar. The $F_{\text{OOC,fossil}}$ values were determined from [14]C
585 analysis of particles collected on filters to allow determination of the fossil fraction of the total
586 carbonaceous material coupled with positive matrix factorization to allow separation of the
587 contributions from the various fossil and non-fossil POA and SOA sources. The uncertainty in the
588 fossil fraction of total OC was reported as 9%; the uncertainty in the $F_{\text{OOC,fossil}}$ will be larger. Zotter
589 et al. (2014) determined the nighttime $F_{\text{OOC,fossil}}$ was smaller than the peak daytime value and that
590 the 24-h average best-estimate $F_{\text{OOC,fossil}} = 44\%$. This is somewhat larger than the average predicted
591 $F_{\text{SOC,fossil}}$ (e.g. 31% for SOM-high). The difference between the observed $F_{\text{OOC,fossil}}$ and predicted
592 $F_{\text{SOC,fossil}}$ could indicate a role for SOA formed from fossil-derived S/IVOC species in the
593 atmosphere but which are not considered here.

4.3.2 The Oxygen-to-Carbon Ratio

595 The O:C atomic ratios of the SOA have been calculated from the simulated distributions of
596 compounds in N_C and N_O space; the O:C atomic ratio is an inherent property of the SOM model
597 and $(O{:}C)_{\text{SOA}}$ values from box model simulations using SOM exhibit generally good agreement
598 with observations (Cappa and Wilson, 2012; Cappa et al., 2013). Few air quality models attempt

20

Deleted: Thus, if there are

Deleted: ratio

Deleted: fossil

Formatted: Font: Italic

Deleted: non-

Deleted: SOA then

Deleted: $F_{\text{OOC,fossil}}$ may not

Deleted: directly comparable

Deleted: F_{SOA}

Deleted: 30

Deleted: F_{SOA}

609   to simulate O:C ratios for SOA (e.g. Murphy et al., 2011), although a dramatic expansion in

610   observations of O:C ratios for ambient OA has recently occurred (Ng et al., 2011; Canagaratna et

611   al., 2015; Chen et al., 2015). Comparison between intensive properties such as O:C, in addition to

612   absolute OA concentrations, can provide further constraints on the transformation processes and

613   OA sources in a given region. The simulated $(O:C)_{SOA}$ in the SOM-no simulations are generally

614   larger in SoCAB than in the eastern US (Figure 6). The simulated $(O:C)_{SOA}$ from isoprene and

615   aromatics individually are larger than those from mono- or sesquiterpenes due, in large part, to the

616   smaller carbon backbone and the need to add more oxygens to produce sufficiently low volatility

617   species that partition substantially to the particle phase (Chhabra et al., 2011; Cappa and Wilson,

618   2012; Tkacik et al., 2012). Thus, the larger $(O:C)_{SOA}$ in SoCAB results from larger relative

619   contributions from isoprene and aromatic compounds to the total SOA burden in this region. The

620    $(O:C)_{SOA}$ is also generally larger in regions where SOA concentrations are smaller. This may

621   reflect some relationship between SOA source and concentration, but it also reflects the role that

622   continued multi-generational oxidation has on the SOA composition, since lower concentrations

623   can reflect greater dilution and overall more aged SOA.

624   The $(O:C)_{SOA}$ for the SOM-low and SOM-high simulations are substantially larger than that

625   from the SOM-no simulations in both SoCAB and the eastern US (Figure 6). This reflects two

626   phenomena: (i) the increased relative contribution of isoprene to the total simulated SOA burden

627   in the SOM-low and SOM-high simulations and (ii) differences in the SOM chemical pathways

628   (i.e. the SOM parameters) that lead to the production of condensed-phase material between the

629   parameterizations that do/do not include vapor wall losses. The influence of the latter has been

630   confirmed through box model simulations, although the exact behavior is both precursor specific

631   and somewhat dependent on the reaction conditions (e.g. [OH] and the initial precursor

632   concentration). Overall, the former effect likely dominates since the difference in simulated

633    $(O:C)_{SOA}$ between isoprene and monoterpenes is substantial (Jathar et al., 2015a).

634   The simulated O:C for the total OA also differs substantially between simulations (Figure 7),

635   especially in regions where the simulated increase in f_{SOA} is largest (Figure 2). The simulated

636    $(O:C)_{total}$ in both the SoCAB and eastern US increases substantially when vapor wall losses are

637   accounted for. For example, the simulated $(O:C)_{total}$ values at Riverside were 0.22, 0.3 and 0.42

638   and at Atlanta were 0.45, 0.65 and 0.85 for SOM-no, SOM-low and SOM-high simulations,

639   respectively. The increase in $(O:C)_{total}$ is mostly driven by an associated increase in f_{SOA}. The

21

640 (O:C)$_{total}$ value is a weighted average of the (O:C)$_{SOA}$ and (O:C)$_{POA}$, with (O:C)$_{total}$ = ($n_{O,SOA}$ +

641 $n_{O,POA}$)/($n_{C,SOA}$ + $n_{C,POA}$) where n_O and n_C indicate the number of oxygen and carbon atoms,

642 respectively, that comprise all SOA types and POA. For conceptual purposes, this exact expression

643 for (O:C)$_{total}$ can be approximated as (O:C)$_{total}$ ~ f_{SOA}(O:C)$_{SOA}$ + (1-f_{SOA})(O:C)$_{POA}$, where (O:C)$_{SOA}$

644 represents the average over the different SOA types. Thus, changes in f_{SOA} lead to changes in

645 (O:C)$_{total}$, with some additional smaller changes due to variation in the weighted average (O:C)$_{SOA}$

646 between the various simulations (since each SOA type has a particular O:C range). The predicted

647 eastern US (O:C)$_{total}$ are generally larger than in SoCAB due to the larger f_{SOA} in the eastern US

648 and since (O:C)$_{SOA}$ is typically larger than (O:C)$_{POA}$. For example, the average (O:C)$_{total}$ in Atlanta

649 for the SOM-no simulations was 0.4 whereas it was 0.22 in Riverside.

650   The simulated results at Riverside can be compared with bulk, campaign average (O:C)$_{total}$

651 values measured during the SOAR campaign using an Aerodyne high resolution time-of-flight

652 aerosol mass spectrometer (HR-AMS), which determines (O:C)$_{total}$ with an absolute uncertainty of

653 ±30% but with very high precision (Docherty et al., 2008; Dzepina et al., 2009). Values reported

654 here have been corrected according to Canagaratna et al. (2015). The campaign-average observed

655 (O:C)$_{total}$ was ~ 0.45. The SOM-high (O:C)$_{total}$ is in very good agreement with the observations,

656 whereas (O:C)$_{total}$ is too small for both SOM-no and SOM-low. This good correspondence is, of

657 course, sensitive to the assumed (O:C)$_{POA}$, here 0.2 based on (Ng et al., 2011). If a smaller (O:C)$_{POA}$

658 had been assumed, then either a greater amount of SOA would be required or the simulated

659 (O:C)$_{SOA}$ would need to be larger to match the SOAR measurements. Docherty et al. (2011)

660 determined there were three POA types during SOAR, with a weighted-average corrected O:C =

661 0.095, suggesting that the assumed 0.2 is too large. In contrast, Hayes et al. (2013) determined a

662 weighted-average corrected O:C = 0.25 for the three POA types identified at Pasadena during

663 CalNex. It has been suggested that at least some of the difference in the (O:C)$_{POA}$ between SOAR

664 and CalNex results from greater heterogeneous ageing of the Pasadena POA. Regardless of the

665 exact (O:C)$_{POA}$, a strong improvement in the model-measurement agreement when vapor wall

666 losses are accounted for is evident. Of additional consideration is the diurnal dependence of the

667 (O:C)$_{total}$. The observed (O:C)$_{total}$ exhibited a distinct diurnal dependence, with low values at night,

668 a minimum at ~7 am and maximum values around midday (Figure 8). The simulated (O:C)$_{total}$

669 diurnal profile for the SOM-high simulations agrees reasonably well with the SOAR observations

670 in terms of both the magnitude of the day-night difference and the absolute (O:C)$_{total}$ (Figure 8). In

22

671 contrast, both the SOM-no and SOM-low exhibit only minor variations with time-of-day due to
672 the controlling influence of $(O:C)_{POA}$.

673 The simulated $(O:C)_{total}$ values in the eastern US can also be compared with recent
674 observations, with the caveat that in this case the measurements were not made over the same time-
675 period as the simulations were run. Nonetheless, measurements made in summer and winter of
676 2012 and 2013 at various locations in Alabama and Georgia indicate the O:C values for total OA
677 were relatively constant, around 0.6-0.7, although it should be noted that these values were
678 estimated from measurements made using an Aerodyne aerosol chemical speciation monitor,
679 which increases the uncertainty (Xu et al., 2015b). Measurements made around the southeast US
680 using an HR-AMS onboard the NASA DC8 as part of the SEAC4RS field study indicate the
681 average $(O:C)_{total} = 0.8$ when the plane was flying below 1 km (SEAC4RS, 2014). As noted above,
682 the simulated $(O:C)_{total}$ around Atlanta was 0.45 for SOM-no, increasing to ~0.65 for SOM-low
683 and ~0.85 for SOM-high. As with the SoCAB comparison, the general level of agreement between
684 the observed and simulated $(O:C)_{tot}$ was improved when vapor wall losses were accounted for.

685 The above simulations included SOA only from VOCs, neglecting contributions from
686 S/IVOCs including oxidation of semi-volatile POA vapors. S/IVOCs and semi-volatile POA
687 vapors are likely $\geq C_{14}$ carbon species (Jathar et al., 2014; Zhao et al., 2014). As such, little added oxygen
688 is required to produce low-volatility species that will form SOA. Since these species also have
689 relatively large number of carbon atoms, the O:C of the SOA formed from them will be relatively
690 small, most likely with $(O:C)_{S/IVOC} < 0.2$ in the absence of strong heterogeneous oxidation (Cappa
691 and Wilson, 2012; Tkacik et al., 2012); note that this range is lower than what was assumed for
692 the non-volatile POA here. Consequently, had S/IVOCs been included in the simulations the
693 $(O:C)_{total}$ would have likely decreased. The magnitude of the decrease would depend on the exact
694 extent to which the S/IVOCs contributed to the overall SOA burden, the extent to which the
695 simulated POA decreased (due to the semi-volatile treatment), and on the simulated $(O:C)_{S/IVOC}$.
696 In the limit that SOA from S/IVOCs dominates the SOA budget, very little variation in the
697 $(O:C)_{total}$ ratio with time of day would have likely been predicted because $(O:C)_{POA} \sim (O:C)_{S/IVOC}$.
698 Additionally, the simulated daytime $(O:C)_{total}$ values would have likely been close to 0.2. A lack
699 of diurnal variability and a small $(O:C)_{total}$ would both be inconsistent with the SOAR observations.
700 Consequently, this implies that accounting for vapor wall losses has a stronger potential to allow
701 for simultaneous reconciliation of the diurnal behavior of both the simulated OA/ΔCO and

23

702 (O:C)$_{total}$ with observations than does consideration of oxidation of S/IVOCs alone. This is not to
703 say that S/IVOC contributions to the SOA and total OA burden are not important, only that it
704 seems unlikely that they could dominate the SOA budget. Ultimately, it seems likely that
705 consideration of both vapor wall losses (as done here) and of SOA from S/IVOCs will be necessary
706 to fully close the model/measurement gap.

707

708 **5 Conclusions**

709   The influence of chamber vapor wall losses on simulated SOA concentrations and properties
710 has been assessed. The statistical oxidation model was used to parameterize SOA formation from
711 laboratory chamber experiments both with and without accounting for vapor wall losses using data
712 from experiments conducted under both high-NO$_x$ and low-NO$_x$ conditions. "Low" and a "high"
713 vapor wall loss cases were considered in addition to the "no" vapor wall loss case. The best-fit
714 SOM parameters under these different conditions were used as input to SOA simulations in the
715 3D UCD/CIT regional air quality model, in which SOM has been recently implemented (Jathar et
716 al., 2015a). Simulations were run for southern California and for the eastern US. Explicit
717 accounting for vapor wall losses led to increases in simulated SOA concentrations, by a factor of
718 ~2-5 for the "low" simulations and ~5-10 for the "high" simulations. The magnitude of the increase
719 was inversely related to the simulated absolute SOA concentration. This suggests that the extent
720 to which SOA concentrations are underpredicted may be greater in more remote regions.

721   This increase in simulated SOA when vapor wall losses are accounted for leads to a substantial
722 increase in the simulated SOA fraction of total OA. This is especially seen in SoCAB where f_{SOA}
723 is very small for the base model but >50% for the simulations that account for vapor wall losses.
724 The simulated f_{SOA} in SoCAB is found to agree reasonably well with observations when vapor wall
725 losses are accounted for. Comparison of the OA/ΔCO from the SoCAB simulations with
726 observations form the SOAR campaign (Docherty et al., 2008) indicate that accounting for vapor
727 wall losses leads to substantially improved agreement in terms of the diurnal behavior, in particular
728 the magnitude of the daytime increase in OA/ΔCO. Accounting for vapor wall losses also leads to
729 location-specific changes in the major contributing VOC precursors to the SOA burden. In general,
730 accounting for vapor wall losses leads to an increase in the predicted relative contribution of
731 isoprene SOA and a decrease in the relative contribution of monoterpene and sesquiterpene SOA.

24

732 The relative contribution of total anthropogenic VOCs to SOA is reasonably insensitive to vapor
733 wall losses, especially in SoCAB, although the apportionment between aromatic VOCs and
734 alkanes does vary with vapor wall losses. The simulated anthropogenic SOA fraction is, however,
735 somewhat smaller than suggested by ^{14}C observations during CalNex (Zotter et al., 2014). In
736 general, the simulated O:C atomic ratio of the SOA increased for the low and high vapor wall loss
737 simulations, compared to the base case. The simulated O:C of the total OA (SOA + POA) in both
738 SoCAB and the eastern US are in better agreement with observations when vapor wall losses are
739 accounted for.

740 Overall, the generally improved model performance when vapor wall losses are accounted
741 for—in terms of both absolute and relative concentrations and in terms of SOA properties—
742 suggests that accounting for this chamber effect in atmospheric simulations of SOA is important,
743 although certainly requiring further examination. Our results qualitatively agree with other recent
744 efforts to assess the influence of vapor wall losses on ambient SOA concentrations (Baker et al.,
745 2015; Hayes et al., 2015), but as our accounting for vapor wall loss is inherent in the SOA
746 parameterization the simulations here serve to provide a more robust assessment. The results
747 presented here additionally suggest that there may be no need to invoke *ad hoc* "ageing" schemes
748 for aromatics (Tsimpidi et al., 2010) to achieve increases in simulated SOA concentrations in urban
749 environments. Further, these results suggest that that the contribution of S/IVOCs to urban SOA
750 might be somewhat limited, albeit still important, although this issue certainly requires further
751 investigation.

752

753 **Author Contributions**

754 The manuscript was written through contributions of all authors. CDC, SHJ, MJK, JHS and
755 ASW designed the project. SHJ and MJK carried out the simulations. CDC determined model
756 parameters using laboratory data collected by JHS. KSD and JLJ collected and processed the
757 SOAR data. All authors have given approval to the final version of the manuscript.

758

759 **Acknowledgements**

25

764

765 References

766 Baker, K. R., Carlton, A. G., Kleindienst, T. E., Offenberg, J. H., Beaver, M. R., Gentner, D. R.,
767 Goldstein, A. H., Hayes, P. L., Jimenez, J. L., Gilman, J. B., de Gouw, J. A., Woody, M. C., Pye,
768 H. O. T., Kelly, J. T., Lewandowski, M., Jaoui, M., Stevens, P. S., Brune, W. H., Lin, Y. H.,
769 Rubitschun, C. L., and Surratt, J. D.: Gas and aerosol carbon in California: comparison of
770 measurements and model predictions in Pasadena and Bakersfield, Atmos. Chem. Phys., 15,
771 5243-5258, doi:10.5194/acp-15-5243-2015, 2015.

772 Budisulistiorini, S. H., Canagaratna, M. R., Croteau, P. L., Marth, W. J., Baumann, K., Edgerton,
773 E. S., Shaw, S. L., Knipping, E. M., Worsnop, D. R., Jayne, J. T., Gold, A., and Surratt, J. D.:
774 Real-Time Continuous Characterization of Secondary Organic Aerosol Derived from Isoprene
775 Epoxydiols in Downtown Atlanta, Georgia, Using the Aerodyne Aerosol Chemical Speciation
776 Monitor, Environ. Sci. Technol., 47, 5686-5694, doi:10.1021/es400023n, 2013.

777 Canagaratna, M. R., Jimenez, J. L., Kroll, J. H., Chen, Q., Kessler, S. H., Massoli, P.,
778 Hildebrandt Ruiz, L., Fortner, E., Williams, L. R., Wilson, K. R., Surratt, J. D., Donahue, N. M.,
779 Jayne, J. T., and Worsnop, D. R.: Elemental ratio measurements of organic compounds using
780 aerosol mass spectrometry: characterization, improved calibration, and implications, Atmos.
781 Chem. Phys., 15, 253-272, doi:10.5194/acp-15-253-2015, 2015.

782 Cappa, C. D. and Wilson, K. R.: Multi-generation gas-phase oxidation, equilibrium partitioning,
783 and the formation and evolution of secondary organic aerosol, Atmos. Chem. Phys., 12, 9505-
784 9528, doi:10.5194/acp-12-9505-2012, 2012.

785 Cappa, C. D., Zhang, X., Loza, C. L., Craven, J. S., Yee, L. D., and Seinfeld, J. H.: Application
786 of the Statistical Oxidation Model (SOM) to secondary organic aerosol formation from
787 photooxidation of C12 Alkanes, Atmos. Chem. Phys., 13, 1591-1606, doi:10.5194/acp-13-1591-
788 2013, 2013.

789 Carlton, A. G., Bhave, P. V., Napelenok, S. L., Edney, E. O., Sarwar, G., Pinder, R. W., Pouliot,
790 G. A., and Houyoux, M.: Model Representation of Secondary Organic Aerosol in CMAQv4.7,
791 Environ. Sci. Technol., 44, 8553-8560, doi:10.1021/es100636q, 2010.

792 Chen, Q., Heald, C. L., Jimenez, J. L., Canagaratna, M. R., Qi, Z., Ling-Yan, H., Xiao-Feng, H.,
793 Campuzano-Jost, P., Palm, B. B., Poulain, L., Kuwata, M., Martin, S. T., Abbatt, J. P. D., Lee,
794 A. K. Y., and Liggio, J.: Elemental composition of organic aerosol: the gap between ambient and
795 laboratory measurements, Geophys. Res. Lett., 42, 4182-4189, doi:10.1002/2015gl063693, 2015.

796 Chhabra, P. S., Ng, N. L., Canagaratna, M. R., Corrigan, A. L., Russell, L. M., Worsnop, D. R.,
797 Flagan, R. C., and Seinfeld, J. H.: Elemental composition and oxidation of chamber organic
798 aerosol, Atmos. Chem. Phys., 11, 8827-8845, doi:10.5194/acp-11-8827-2011, 2011.

26

799   De Gouw, J. and Jimenez, J. L.: Organic Aerosols in the Earth's Atmosphere, Environ. Sci.
800   Technol., 43, 7614-7618, doi:10.1021/es9006004, 2009.

801   Docherty, K. S., Aiken, A. C., Huffman, J. A., Ulbrich, I. M., DeCarlo, P. F., Sueper, D.,
802   Worsnop, D. R., Snyder, D. C., Peltier, R. E., Weber, R. J., Grover, B. D., Eatough, D. J.,
803   Williams, B. J., Goldstein, A. H., Ziemann, P. J., and Jimenez, J. L.: The 2005 Study of Organic
804   Aerosols at Riverside (SOAR-1): instrumental intercomparisons and fine particle composition,
805   Atmos. Chem. Phys., 11, 12387-12420, doi:10.5194/acp-11-12387-2011, 2011.

806   Docherty, K. S., Stone, E. A., Ulbrich, I. M., DeCarlo, P. F., Snyder, D. C., Schauer, J. J., Peltier,
807   R. E., Weber, R. J., Murphy, S. M., Seinfeld, J. H., Grover, B. D., Eatough, D. J., and Jimenez, J.
808   L.: Apportionment of Primary and Secondary Organic Aerosols in Southern California during
809   the 2005 Study of Organic Aerosols in Riverside (SOAR-1), Environ. Sci. Technol., 42, 7655-
810   7662, doi:10.1021/es8008166, 2008.

811   Dzepina, K., Cappa, C. D., Volkamer, R. M., Madronich, S., DeCarlo, P. F., Zaveri, R. A., and
812   Jimenez, J. L.: Modeling the Multiday Evolution and Aging of Secondary Organic Aerosol
813   During MILAGRO 2006, Environ. Sci. Technol., 45, 3496-3503, doi:10.1021/es103186f, 2011.

814   Dzepina, K., Volkamer, R. M., Madronich, S., Tulet, P., Ulbrich, I. M., Zhang, Q., Cappa, C. D.,
815   Ziemann, P. J., and Jimenez, J. L.: Evaluation of recently-proposed secondary organic aerosol
816   models for a case study in Mexico City, Atmos. Chem. Phys., 9, 5681-5709, doi:10.5194/acp-9-
817   5681-2009, 2009.

818   Ensberg, J. J., Hayes, P. L., Jimenez, J. L., Gilman, J. B., Kuster, W. C., de Gouw, J. A.,
819   Holloway, J. S., Gordon, T. D., Jathar, S. H., Robinson, A. L., and Seinfeld, J. H.: Emission
820   factor ratios, SOA mass yields, and the impact of vehicular emissions on SOA formation, Atmos.
821   Chem. Phys., 14, 2383-2397, doi:10.5194/acp-14-2383-2014, 2013.

822   Ervens, B., Turpin, B. J., and Weber, R. J.: Secondary organic aerosol formation in cloud
823   droplets and aqueous particles (aqSOA): a review of laboratory, field and model studies, Atmos.
824   Chem. Phys., 11, 11069-11102, doi:10.5194/acp-11-11069-2011, 2011.

825   Hayes, P. L., Carlton, A. G., Baker, K. R., Ahmadov, R., Washenfelder, R. A., Alvarez, S.,
826   Rappenglück, B., Gilman, J. B., Kuster, W. C., de Gouw, J. A., Zotter, P., Prévôt, A. S. H.,
827   Szidat, S., Kleindienst, T. E., Offenberg, J. H., and Jimenez, J. L.: Modeling the formation and
828   aging of secondary organic aerosols in Los Angeles during CalNex 2010, Atmos. Chem. Phys.,
829   15, 5773-5801, doi:10.5194/acp-15-5773-2015, 2015.

830   Hayes, P. L., Ortega, A. M., Cubison, M. J., Froyd, K. D., Zhao, Y., Cliff, S. S., Hu, W. W.,
831   Toohey, D. W., Flynn, J. H., Lefer, B. L., Grossberg, N., Alvarez, S., Rappenglück, B., Taylor, J.
832   W., Allan, J. D., Holloway, J. S., Gilman, J. B., Kuster, W. C., de Gouw, J. A., Massoli, P.,
833   Zhang, X., Liu, J., Weber, R. J., Corrigan, A. L., Russell, L. M., Isaacman, G., Worton, D. R.,
834   Kreisberg, N. M., Goldstein, A. H., Thalman, R., Waxman, E. M., Volkamer, R., Lin, Y. H.,
835   Surratt, J. D., Kleindienst, T. E., Offenberg, J. H., Dusanter, S., Griffith, S., Stevens, P. S.,
836   Brioude, J., Angevine, W. M., and Jimenez, J. L.: Organic aerosol composition and sources in
837   Pasadena, California, during the 2010 CalNex campaign, J. Geophys. Res.-Atmos., 118, 9233-
838   9257, doi:10.1002/jgrd.50530, 2013.

839   Heald, C. L., Jacob, D. J., Park, R. J., Russell, L. M., Huebert, B. J., Seinfeld, J. H., Liao, H., and
840   Weber, R. J.: A large organic aerosol source in the free troposphere missing from current
841   models, Geophys. Res. Lett., 32, L18809, doi:10.1029/2005GL023831, 2005.

842 Hodzic, A., Aumont, B., Knote, C., Lee-Taylor, J., Madronich, S., and Tyndall, G.: Volatility
843 dependence of Henry's law constants of condensable organics: Application to estimate
844 depositional loss of secondary organic aerosols, Geophys. Res. Lett., 41, 4795-4804,
845 doi:10.1002/2014gl060649, 2014.

846 Hodzic, A., Kasibhatla, P. S., Jo, D. S., Cappa, C. D., Jimenez, J. L., Madronich, S., and Park, R.
847 J.: Rethinking the global secondary organic aerosol (SOA) budget: stronger production, faster
848 removal, shorter lifetime, Atmos. Chem. Phys. Discuss., Submitted. Submitted.

849 Hu, W. W., Campuzano-Jost, P., Palm, B. B., Day, D. A., Ortega, A. M., Hayes, P. L.,
850 Krechmer, J. E., Chen, Q., Kuwata, M., Liu, Y. J., de Sá, S. S., Martin, S. T., Hu, M.,
851 Budisulistiorini, S. H., Riva, M., Surratt, J. D., St. Clair, J. M., Isaacman-Van Wertz, G., Yee, L.
852 D., Goldstein, A. H., Carbone, S., Artaxo, P., de Gouw, J. A., Koss, A., Wisthaler, A., Mikoviny,
853 T., Karl, T., Kaser, L., Jud, W., Hansel, A., Docherty, K. S., Robinson, N. H., Coe, H., Allan, J.
854 D., Canagaratna, M. R., Paulot, F., and Jimenez, J. L.: Characterization of a real-time tracer for
855 Isoprene Epoxydiols-derived Secondary Organic Aerosol (IEPOX-SOA) from aerosol mass
856 spectrometer measurements, Atmos. Chem. Phys. Discuss., 15, 11223-11276, doi:10.5194/acpd-
857 15-11223-2015, 2015.

858 Jathar, S. H., Cappa, C. D., Wexler, A. S., Seinfeld, J. H., and Kleeman, M. J.: Multi-
859 generational Oxidation Model to Simulate Secondary Organic Aerosol in a 3D Air Quality
860 Model, Geosci. Model Dev., 8, 2553-2567, doi:10.5194/gmd-8-2553-2015, 2015a.

861 Jathar, S. H., Cappa, C. D., Wexler, A. S., Seinfeld, J. H., and Kleeman, M. J.: Simulating
862 secondary organic aerosol in a regional air quality model using the statistical oxidation model –
863 Part 1: Assessing the influence of constrained multi-generational ageing, Atmos. Chem. Phys.
864 Discuss., 15, 25837-25872, doi:10.5194/acpd-15-25837-2015, 2015b.

865 Jathar, S. H., Gordon, T. D., Hennigan, C. J., Pye, H. O. T., Pouliot, G., Adams, P. J., Donahue,
866 N. M., and Robinson, A. L.: Unspeciated organic emissions from combustion sources and their
867 influence on the secondary organic aerosol budget in the United States, Proc. Nat. Acad. Sci.,
868 111, 10473-10478, doi:10.1073/pnas.1323740111, 2014.

869 Kim, P. S., Jacob, D. J., Fisher, J. A., Travis, K., Yu, K., Zhu, L., Yantosca, R. M., Sulprizio, M.
870 P., Jimenez, J. L., Campuzano-Jost, P., Froyd, K. D., Liao, J., Hair, J. W., Fenn, M. A., Butler, C.
871 F., Wagner, N. L., Gordon, T. D., Welti, A., Wennberg, P. O., Crounse, J. D., St. Clair, J. M.,
872 Teng, A. P., Millet, D. B., Schwarz, J. P., Markovic, M. Z., and Perring, A. E.: Sources,
873 seasonality, and trends of southeast US aerosol: an integrated analysis of surface, aircraft, and
874 satellite observations with the GEOS-Chem chemical transport model, Atmos. Chem. Phys., 15,
875 10411-10433, doi:10.5194/acp-15-10411-2015, 2015.

876 Kleeman, M. J. and Cass, G. R.: A 3D Eulerian Source-Oriented Model for an Externally Mixed
877 Aerosol, Environ. Sci. Technol., 35, 4834-4848, doi:10.1021/es010886m, 2001.

878 Kokkola, H., Yli-Pirilä, P., Vesterinen, M., Korhonen, H., Keskinen, H., Romakkaniemi, S.,
879 Hao, L., Kortelainen, A., Joutsensaari, J., Worsnop, D. R., Virtanen, A., and Lehtinen, K. E. J.:
880 The role of low volatile organics on secondary organic aerosol formation, Atmos. Chem. Phys.,
881 14, 1689-1700, doi:10.5194/acp-14-1689-2014, 2014.

882 Krechmer, J. E., Coggon, M. M., Massoli, P., Nguyen, T. B., Crounse, J. D., Hu, W., Day, D. A.,
883 Tyndall, G. S., Henze, D. K., Rivera-Rios, J. C., Nowak, J. B., Kimmel, J. R., Mauldin, R. L.,
884 Stark, H., Jayne, J. T., Sipilä, M., Junninen, H., Clair, J. M. S., Zhang, X., Feiner, P. A., Zhang,

L., Miller, D. O., Brune, W. H., Keutsch, F. N., Wennberg, P. O., Seinfeld, J. H., Worsnop, D. R., Jimenez, J. L., and Canagaratna, M. R.: Formation of Low Volatility Organic Compounds and Secondary Organic Aerosol from Isoprene Hydroxyhydroperoxide Low-NO Oxidation, Environ. Sci. Technol., 49, 10330-10339, doi:10.1021/acs.est.5b02031, 2015.

Lane, T. E., Donahue, N. M., and Pandis, S. N.: Effect of NOx on Secondary Organic Aerosol Concentrations, Environ. Sci. Technol., 42, 6022-6027, doi:10.1021/es703225a, 2008a.

Lane, T. E., Donahue, N. M., and Pandis, S. N.: Simulating secondary organic aerosol formation using the volatility basis-set approach in a chemical transport model, Atmos. Environ., 42, 7439-7451, doi:10.1016/j.atmosenv.2008.06.026, 2008b.

Matsunaga, A. and Ziemann, P. J.: Gas-Wall Partitioning of Organic Compounds in a Teflon Film Chamber and Potential Effects on Reaction Product and Aerosol Yield Measurements, Aerosol Sci. Technol., 44, 881-892, doi:10.1080/02786826.2010.501044, 2010.

McVay, R. C., Cappa, C. D., and Seinfeld, J. H.: Vapor–Wall Deposition in Chambers: Theoretical Considerations, Environ. Sci. Technol., 48, 10251-10258, doi:10.1021/es502170j, 2014.

Murphy, B. N., Donahue, N. M., Fountoukis, C., and Pandis, S. N.: Simulating the oxygen content of ambient organic aerosol with the 2D volatility basis set, Atmos. Chem. Phys., 11, 7859-7873, doi:10.5194/acp-11-7859-2011, 2011.

Ng, N. L., Canagaratna, M. R., Jimenez, J. L., Chhabra, P. S., Seinfeld, J. H., and Worsnop, D. R.: Changes in organic aerosol composition with aging inferred from aerosol mass spectra, Atmos. Chem. Phys., 11, 6465-6474, doi:10.5194/acp-11-6465-2011, 2011.

Ng, N. L., Chhabra, P. S., Chan, A. W. H., Surratt, J. D., Kroll, J. H., Kwan, A. J., McCabe, D. C., Wennberg, P. O., Sorooshian, A., Murphy, S. M., Dalleska, N. F., Flagan, R. C., and Seinfeld, J. H.: Effect of NOx level on secondary organic aerosol (SOA) formation from the photooxidation of terpenes, Atmos. Chem. Phys., 7, 5159-5174, doi:10.5194/acp-7-5159-2007, 2007a.

Ng, N. L., Kroll, J. H., Chan, A. W. H., Chhabra, P. S., Flagan, R. C., and Seinfeld, J. H.: Secondary organic aerosol formation from m-xylene, toluene, and benzene, Atmos. Chem. Phys., 7, 3909-3922, doi:10.5194/acp-7-3909-2007, 2007b.

Odum, J. R., Hoffmann, T., Bowman, F., Collins, D., Flagan, R. C., and Seinfeld, J. H.: Gas/particle partitioning and secondary organic aerosol yields, Environ. Sci. Technol., 30, 2580-2585, doi:10.1021/es950943+, 1996.

Pankow, J. F.: An absorption-model of the gas aerosol partitioning involved in the formation of secondary organic aerosol, Atmos. Environ., 28, 189-193, doi:10.1016/1352-2310(94)90094-9, 1994.

Pye, H. O. T., Pinder, R. W., Piletic, I. R., Xie, Y., Capps, S. L., Lin, Y.-H., Surratt, J. D., Zhang, Z., Gold, A., Luecken, D. J., Hutzell, W. T., Jaoui, M., Offenberg, J. H., Kleindienst, T. E., Lewandowski, M., and Edney, E. O.: Epoxide Pathways Improve Model Predictions of Isoprene Markers and Reveal Key Role of Acidity in Aerosol Formation, Environ. Sci. Technol., 47, 11056-11064, doi:10.1021/es402106h, 2013.

29

925 Robinson, A. L., Donahue, N. M., Shrivastava, M. K., Weitkamp, E. A., Sage, A. M., Grieshop,
926 A. P., Lane, T. E., Pierce, J. R., and Pandis, S. N.: Rethinking organic aerosols: Semivolatile
927 emissions and photochemical aging, Science, 315, 1259-1262, doi:10.1126/science.1133061,
928 2007.

929 Russell, A. R., Valin, L. C., and Cohen, R. C.: Trends in OMI NO2 observations over the United
930 States: effects of emission control technology and the economic recession, Atmos. Chem. Phys.,
931 12, 12197-12209, doi:10.5194/acp-12-12197-2012, 2012.

932 SEAC4RS: Studies of Emissions and Atmospheric Composition, Clouds and Climate Coupling
933 by Regional Surveys, doi: 10.5067/Aircraft/SEAC4RS/Aerosol-TraceGas-Cloud, 2014. 2014.

934 Simon, H. and Bhave, P. V.: Simulating the Degree of Oxidation in Atmospheric Organic
935 Particles, Environ. Sci. Technol., 46, 331-339, doi:10.1021/es202361w, 2011.

936 Subramanian, R., Khlystov, A. Y., Cabada, J. C., and Robinson, A. L.: Positive and Negative
937 Artifacts in Particulate Organic Carbon Measurements with Denuded and Undenuded Sampler
938 Configurations, Aerosol Sci. Technol., 38, 27-48, doi:10.1080/02786820390229354, 2004.

939 The Visibility Information Exchange Web System (VIEWS 2.0): The Visibility Information
940 Exchange Web System, http://views.cira.colostate.edu/web/, Colorado State University, last
941 access: 11 February 2015, 2015.

942 Tkacik, D. S., Presto, A. A., Donahue, N. M., and Robinson, A. L.: Secondary Organic Aerosol
943 Formation from Intermediate-Volatility Organic Compounds: Cyclic, Linear, and Branched
944 Alkanes, Environ. Sci. Technol., 46, 8773-8781, doi:10.1021/es301112c, 2012.

945 Tsigaridis, K., Daskalakis, N., Kanakidou, M., Adams, P. J., Artaxo, P., Bahadur, R., Balkanski,
946 Y., Bauer, S. E., Bellouin, N., Benedetti, A., Bergman, T., Berntsen, T. K., Beukes, J. P., Bian,
947 H., Carslaw, K. S., Chin, M., Curci, G., Diehl, T., Easter, R. C., Ghan, S. J., Gong, S. L., Hodzic,
948 A., Hoyle, C. R., Iversen, T., Jathar, S., Jimenez, J. L., Kaiser, J. W., Kirkevåg, A., Koch, D.,
949 Kokkola, H., Lee, Y. H., Lin, G., Liu, X., Luo, G., Ma, X., Mann, G. W., Mihalopoulos, N.,
950 Morcrette, J. J., Müller, J. F., Myhre, G., Myriokefalitakis, S., Ng, N. L., O'Donnell, D., Penner,
951 J. E., Pozzoli, L., Pringle, K. J., Russell, L. M., Schulz, M., Sciare, J., Seland, Ø., Shindell, D. T.,
952 Sillman, S., Skeie, R. B., Spracklen, D., Stavrakou, T., Steenrod, S. D., Takemura, T., Tiitta, P.,
953 Tilmes, S., Tost, H., van Noije, T., van Zyl, P. G., von Salzen, K., Yu, F., Wang, Z., Wang, Z.,
954 Zaveri, R. A., Zhang, H., Zhang, K., Zhang, Q., and Zhang, X.: The AeroCom evaluation and
955 intercomparison of organic aerosol in global models, Atmos. Chem. Phys., 14, 10845-10895,
956 doi:10.5194/acp-14-10845-2014, 2014.

957 Tsimpidi, A. P., Karydis, V. A., Zavala, M., Lei, W., Molina, L. T., Ulbrich, I., Jimenez, J. L.,
958 and Pandis, S. N.: Evaluation of the volatility basis-set approach for the simulation of organic
959 aerosol formation in the Mexico City metropolitan area, Atmos. Chem. Phys., 10, 525-546,
960 doi:10.5194/acp-10-525-2010, 2010.

961 Turpin, B. J. and Lim, H.-J.: Species Contributions to PM2.5 Mass Concentrations: Revisiting
962 Common Assumptions for Estimating Organic Mass, Aerosol Sci. Technol., 35, 602-610,
963 doi:10.1080/02786820119445, 2001.

964 Volkamer, R., Jimenez, J. L., San Martini, F., Dzepina, K., Zhang, Q., Salcedo, D., Molina, L.
965 T., Worsnop, D. R., and Molina, M. J.: Secondary organic aerosol formation from anthropogenic

air pollution: Rapid and higher than expected, Geophys. Res. Lett., 33, L17811, doi:10.1029/2006gl026899, 2006.

Worton, D. R., Surratt, J. D., LaFranchi, B. W., Chan, A. W. H., Zhao, Y., Weber, R. J., Park, J.-H., Gilman, J. B., de Gouw, J., Park, C., Schade, G., Beaver, M., Clair, J. M. S., Crounse, J., Wennberg, P., Wolfe, G. M., Harrold, S., Thornton, J. A., Farmer, D. K., Docherty, K. S., Cubison, M. J., Jimenez, J.-L., Frossard, A. A., Russell, L. M., Kristensen, K., Glasius, M., Mao, J., Ren, X., Brune, W., Browne, E. C., Pusede, S. E., Cohen, R. C., Seinfeld, J. H., and Goldstein, A. H.: Observational Insights into Aerosol Formation from Isoprene, Environ. Sci. Technol., 47, 11403-11413, doi:10.1021/es4011064, 2013.

Xu, L., Guo, H., Boyd, C. M., Klein, M., Bougiatioti, A., Cerully, K. M., Hite, J. R., Isaacman-VanWertz, G., Kreisberg, N. M., Knote, C., Olson, K., Koss, A., Goldstein, A. H., Hering, S. V., de Gouw, J., Baumann, K., Lee, S.-H., Nenes, A., Weber, R. J., and Ng, N. L.: Effects of anthropogenic emissions on aerosol formation from isoprene and monoterpenes in the southeastern United States, Proc. Nat. Acad. Sci., 112, 37-42, doi:10.1073/pnas.1417609112, 2015a.

Xu, L., Kollman, M. S., Song, C., Shilling, J. E., and Ng, N. L.: Effects of NOx on the Volatility of Secondary Organic Aerosol from Isoprene Photooxidation, Environ. Sci. Technol., 48, 2253-2262, doi:10.1021/es404842g, 2014.

Xu, L., Suresh, S., Guo, H., Weber, R. J., and Ng, N. L.: Aerosol characterization over the southeastern United States using high-resolution aerosol mass spectrometry: spatial and seasonal variation of aerosol composition and sources with a focus on organic nitrates, Atmos. Chem. Phys., 15, 7307-7336, doi:10.5194/acp-15-7307-2015, 2015b.

Yeh, G. K. and Ziemann, P. J.: Gas-wall partitioning of oxygenated organic compounds: Measurements, structure-activity relationships, and correlation with gas chromatographic retention factor, Aerosol Sci. Technol., 49, 727-738, doi:10.1080/02786826.2015.1068427, 2015.

Zhang, Q., Jimenez, J. L., Canagaratna, M. R., Allan, J. D., Coe, H., Ulbrich, I., Alfarra, M. R., Takami, A., Middlebrook, A. M., Sun, Y. L., Dzepina, K., Dunlea, E., Docherty, K., DeCarlo, P. F., Salcedo, D., Onasch, T., Jayne, J. T., Miyoshi, T., Shimono, A., Hatakeyama, S., Takegawa, N., Kondo, Y., Schneider, J., Drewnick, F., Borrmann, S., Weimer, S., Demerjian, K., Williams, P., Bower, K., Bahreini, R., Cottrell, L., Griffin, R. J., Rautiainen, J., Sun, J. Y., Zhang, Y. M., and Worsnop, D. R.: Ubiquity and dominance of oxygenated species in organic aerosols in anthropogenically-influenced Northern Hemisphere midlatitudes, Geophysical Research Letters, 34, L13801, doi:10.1029/2007GL029979, 2007.

Zhang, X., Cappa, C. D., Jathar, S. H., McVay, R. C., Ensberg, J. J., Kleeman, M. J., and Seinfeld, J. H.: Influence of vapor wall loss in laboratory chambers on yields of secondary organic aerosol, Proc. Nat. Acad. Sci., 111, 5802-5807, doi:10.1073/pnas.1404727111, 2014.

Zhang, X., Schwantes, R. H., McVay, R. C., Lignell, H., Coggon, M. M., Flagan, R. C., and Seinfeld, J. H.: Vapor wall deposition in Teflon chambers, Atmos. Chem. Phys., 15, 4197-4214, doi:10.5194/acp-15-4197-2015, 2015.

Zhao, Y., Hennigan, C. J., May, A. A., Tkacik, D. S., de Gouw, J. A., Gilman, J. B., Kuster, W. C., Borbon, A., and Robinson, A. L.: Intermediate-Volatility Organic Compounds: A Large

1008   Source of Secondary Organic Aerosol, Environ. Sci. Technol., 48, 13743-13750,
1009   doi:10.1021/es5035188, 2014.

1010   Ziemann, P. J. and Atkinson, R.: Kinetics, products, and mechanisms of secondary organic
1011   aerosol formation, Chem. Soc. Rev., 41, 6582-6605, doi:10.1039/C2CS35122F, 2012.

1012   Zotter, P., El-Haddad, I., Zhang, Y., Hayes, P. L., Zhang, X., Lin, Y.-H., Wacker, L., Schnelle-
1013   Kreis, J., Abbaszade, G., Zimmermann, R., Surratt, J. D., Weber, R., Jimenez, J. L., Szidat, S.,
1014   Baltensperger, U., and Prévôt, A. S. H.: Diurnal cycle of fossil and nonfossil carbon using
1015   radiocarbon analyses during CalNex, J. Geophys. Res.-Atmos., 119, 6818-6835,
1016   doi:10.1002/2013JD021114, 2014.

1017

32

1018 **Table 1.** Model performance metrics determined for the three simulation groupings (SOM-no, SOM-low and SOM-high) for the low-
1019 NO$_x$, high-NO$_x$ and average parameterizations for STN and IMPROVE sites in SoCAB and the eastern US. Fractional bias is calculated
1020 as $2(C_{OA,sim}-C_{OA,obs})/(C_{OA,sim}+C_{OA,obs})$ and NMSE as $abs[(C_{OA,sim}-C_{OA,obs})^2/(C_{OA,sim}\times C_{OA,obs})]$, and the reported values are the averages
1021 over all data points as percentages. Note that a negative fractional bias indicates observed [SOA] > simulated [SOA], i.e. that the
1022 simulations are underpredicting. ρ_c are the concordance correlation coefficients from Eqn. 3.

1023

Simulation	NO$_x$ parameterization	Southern California						Eastern US					
		STN[a]			IMPROVE[b]			STN[a]			IMPROVE[b,c]		
		Frac. Bias	NMSE	ρ_c	Frac. Bias	NMSE	ρ_c	Frac. Bias	NMSE	ρ_c	Frac. Bias	NMSE	ρ_c
SOM-no	low	-70	88	0.03	-75	114	0.36	-81	206	0.04	-55	105	0.31
	high	-61	69	0.02	-60	85	0.41	-58	166	0.12	-24	84	0.48
	average	-65	78	0.02	-67	97	0.39	-68	180	0.08	-38	89	0.43
SOM-low	low	-52	64	-0.21	-45	65	0.36	-26	154	0.08	15	85	0.15
	high	-39	49	-0.29	-27	47	0.27	-4	171	0.07	38	128	0.10
	average	-45	55	-0.25	-36	54	0.32	-14	160	0.08	28	105	0.12
SOM-high	low	-25	51	-0.03	-8	46	0.44	26	236	0.15	69	189	0.40
	high	-10	38	-0.08	16	43	0.46	45	298	0.15	86	295	0.25
	average	-17	43	-0.05	5	42	0.46	36	265	0.16	79	241	0.31

[a] Observed [OA] for STN sites estimated as 1.6([OC] – 0.5 μg m^{-3})

[b] Observed [OA] for IMPROVE sites estimated as 2.1[OC].

[c] Observed [OA] may be biased low by ~25% in the SE US summer due to evaporation after sampling (Kim et al., 2015).

1024

1025

33

1030
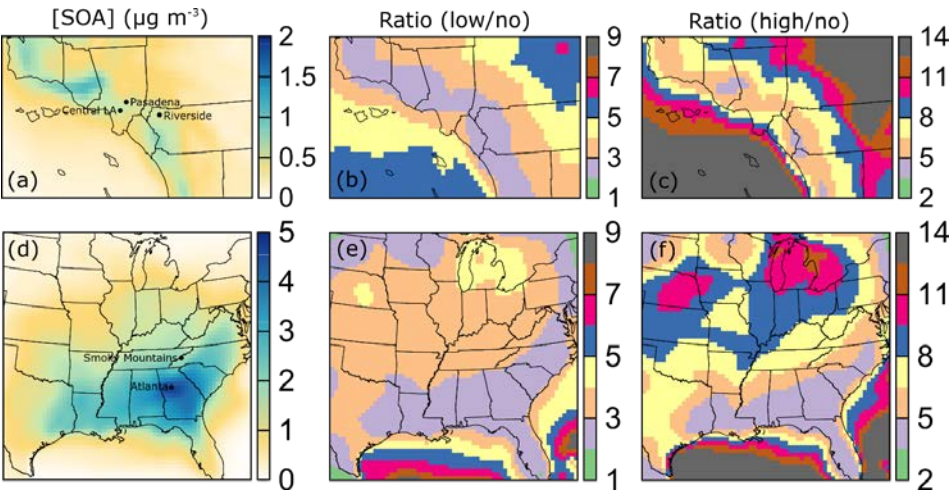
1031

1032 **Figure 1.** 14-day averaged SOA concentrations, in μg m⁻³, for (a) SoCAB and (d) the eastern US
1033 for the SOM-no simulations. The averaging time periods are from July 20th to August 2nd, 2005
1034 for SoCAB and from August 20th to September 2nd, 2006 for the eastern US. Panels (b,e) show the
1035 ratio between the SOA concentrations for the SOM-low and the SOM-no simulations and Panels
1036 (c,f) show the ratio between the SOM-high and SOM-no simulations. Results shown in all panels
1037 are the average of the low- and high-NOx simulations. Note that the color scale for the absolute
1038 SOA concentration is continuous whereas the color scale in the ratio plots is discrete.

1039

1040

34

1041
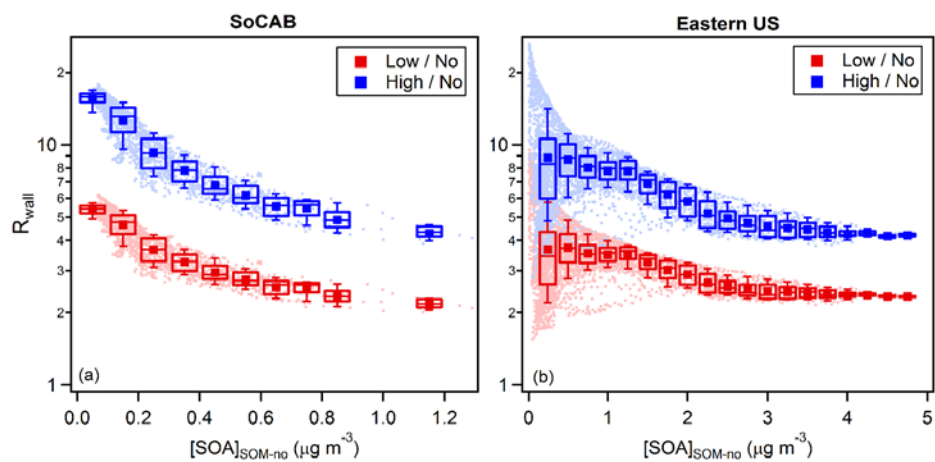
1042

Figure 2. Variation of the ratio between simulated SOA concentrations from SOM-low (red) and
SOM-high (blue) simulations to SOM-no simulations for (a) SoCAB and (b) the eastern US as a
function of the absolute SOA concentration from the SOM-no simulations. Results shown are the
average of the low- and high-NO_x simulations. Individual data points are shown along with box
and whisker plots.

1048
1049

1050
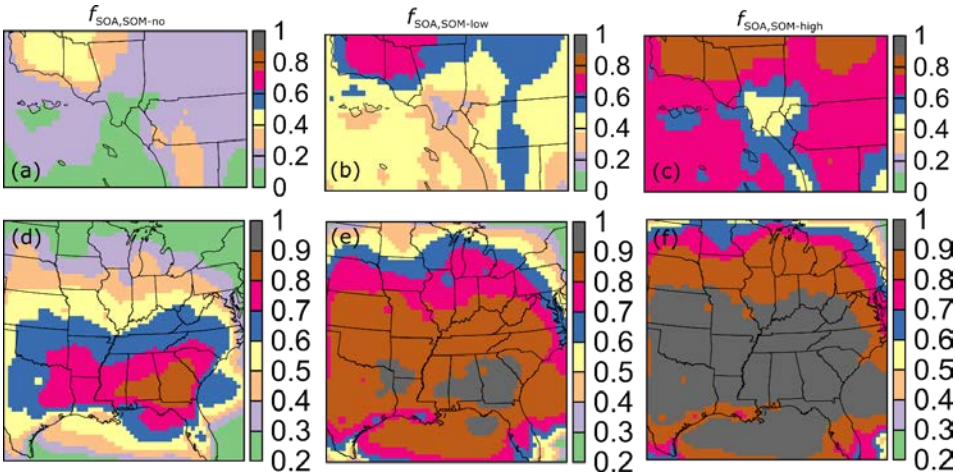
1051

Figure 3. 14-day averaged f_{SOA}, the ratio between SOA and total OA concentrations, for (top panels, a, b, c) SoCAB and (bottom panels, d, e, f) the eastern US for the (a, d) SOM-no, (b, e) SOM-low and (c, f) SOM-high simulations.

1055

1056

1057
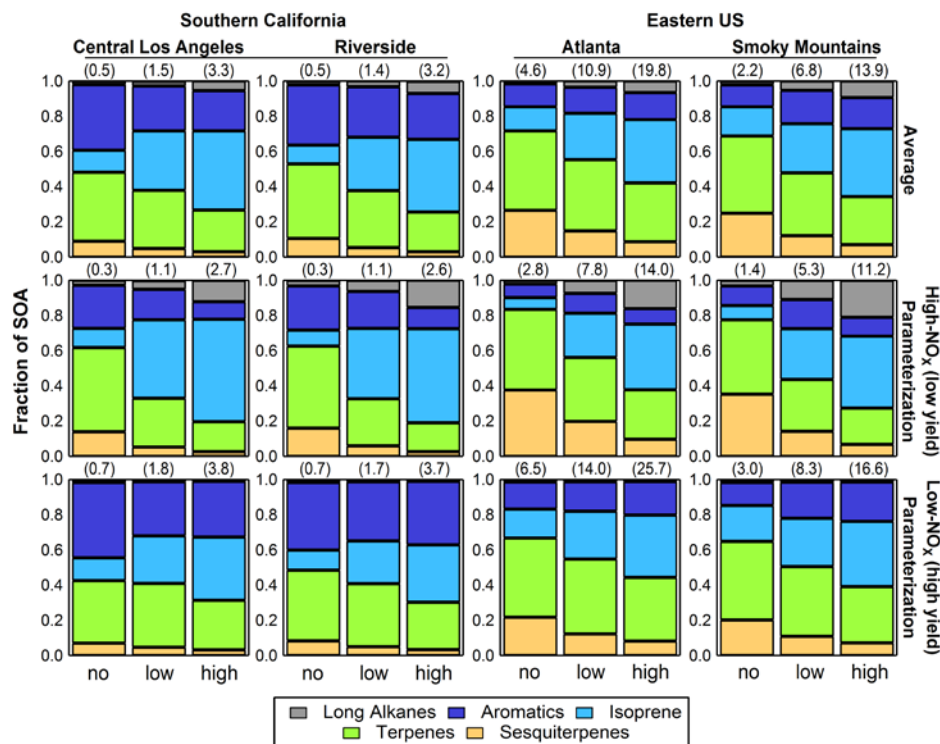
Figure 4. Bar charts showing the fractional contribution from the various VOC precursor classes to the total simulated SOA for two locations in SoCAB (central Los Angeles and Riverside) and two in the eastern US (Atlanta and the Smoky Mountains). Results are shown for (top) average, (middle) high-NO_x, low-yield and (bottom) low-NO_x, high-yield simulations. Each panel shows results from the 14-day average (left-to-right) SOM-no, SOM-low and SOM-high simulations. The average SOA concentration (in $\mu g\ m^{-3}$) is for each location and simulation is given in parentheses above each panel.

37

1067
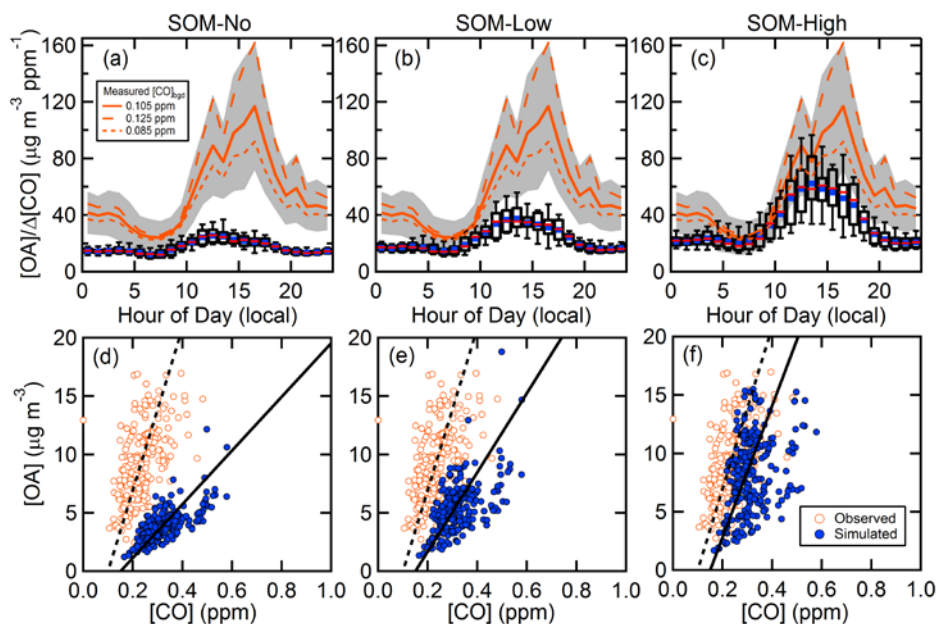
Figure 5. Simulated and observed diurnal profiles for the OA/ΔCO ratio (top panels) at Riverside, CA during the SOAR-2005 campaign for (a) SOM-no, (b) SOM-low and (c) SOM-high simulations. For the observations, the mean (solid orange line) and the 1σ variability range (grey band) are shown for $[CO]_{bgd} = 0.105$ ppm, and only mean values are shown for $[CO]_{bgd} = 0.085$ ppm (short dashed orange line) and $[CO]_{bgd} = 0.125$ ppm (long dashed orange line). For the simulations, box and whisker plots are shown with the median (red –), mean (blue squares), lower and upper quartile (boxes), and 9th and 91st percentile (whiskers). The bottom panels (e-f) show scatter plots of [OA] versus [CO] for both the ambient measurements (open orange circles) and for the model results (blue circles) for daytime hours (10 am – 8 pm). The lines are linear fits where the x-axis intercept has been constrained to go through the assumed $[CO]_{bgd}$ (dashed = observed; solid = model). The derived slopes are 69 ± 2 (observed), 23.0 ± 0.4 (SOM-no), 34.0 ± 0.8 (SOM-low) and 55 ± 2 (SOM-high) μg m^{-3} ppm^{-1} and where the uncertainties are fit errors.

1080
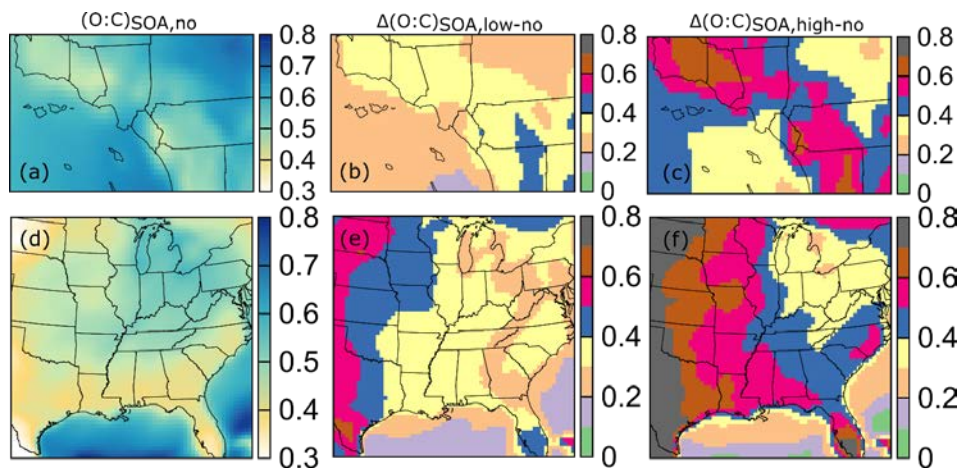
Figure 6. 14-day averaged O:C atomic ratios for SOA for (a) SoCAB and (d) the eastern US for the SOM-no simulations. The difference in O:C between the SOM-low or SOM-high and SOM-no simulations, termed Δ(O:C), is shown in panels (b-c) for SoCAB and (e-f) for the eastern US.

1086
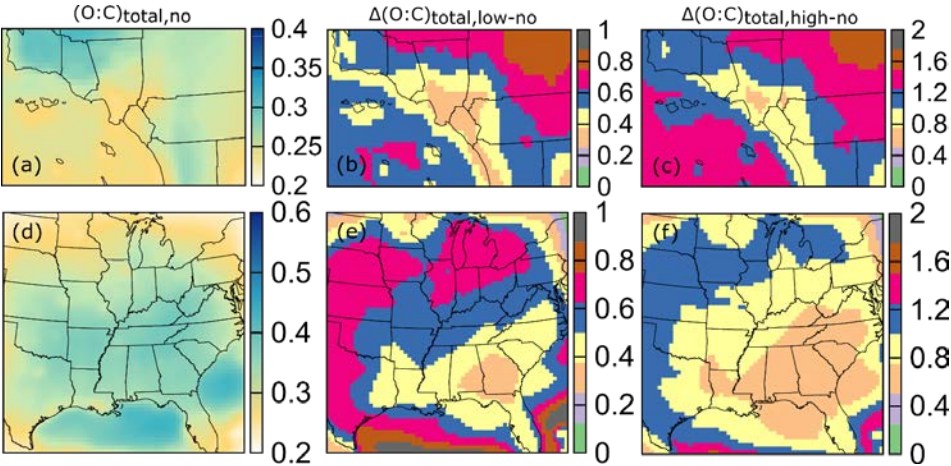
1087

Figure 7. 14-day averaged O:C atomic ratios for total OA (POA + SOA) for (a) SoCAB and (d)
the eastern US for the SOM-no simulations. The normalized difference in O:C, Δ(O:C), between
the SOM-low or SOM-high and SOM-no simulations, where Δ(O:C) is defined as
$((O:C)_{SOM-low/high}-(O:C)_{SOM-no})/(O:C)_{SOM-no})$, is shown in panels (b-c) for SoCAB and (e-f) for the
eastern US. In all cases, the O:C for POA was assumed to be 0.2.

1093

40

1094
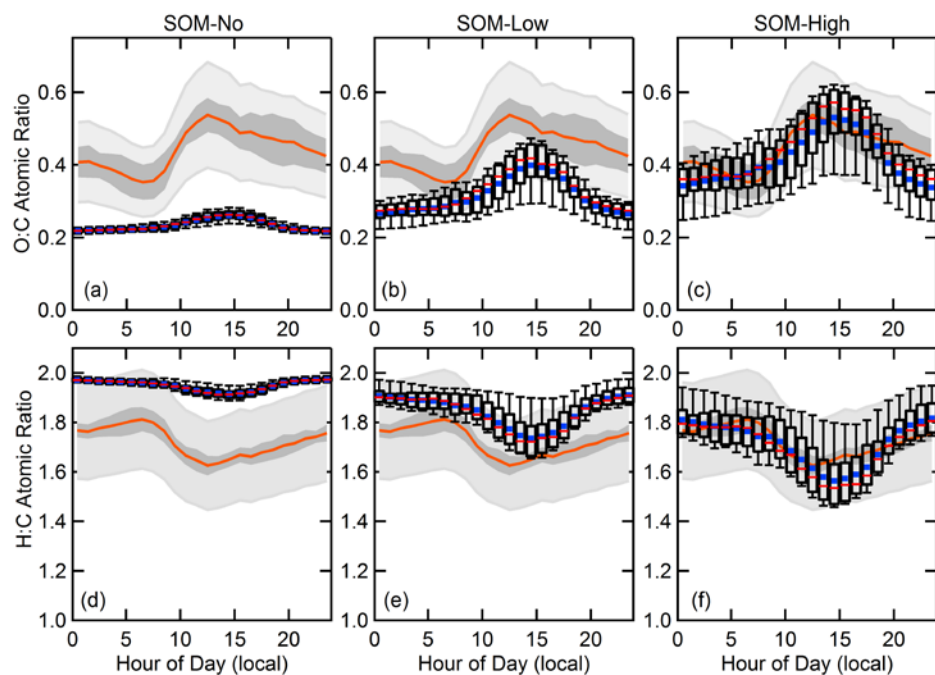
1095

Figure 8. Simulated and observed diurnal profiles for the total OA O:C (panels a, b, c) and H:C (panels d, e, f) atomic ratios at Riverside, CA during the SOAR-2005 campaign for (a, d) SOM-no, (b, e) SOM-low and (c, f) SOM-high simulations. For the observations, the mean (orange line) and the 1σ variability range (dark grey band) are shown along with bands indicating the measurement uncertainty (light grey band), taken as ± 28% for O:C and 13% for H:C (Canagaratna et al., 2015). Observed values have been corrected according to Canagaratna et al. (2015). For the simulations, box and whisker plots are shown with the median (red –), lower and upper quartile (boxes), and 9th and 91st percentile (whiskers). For reference, the assumed O:C for POA was 0.2 and for H:C was 2.0.

1105

41

The Supplemental Material consists of five figures and two tables.
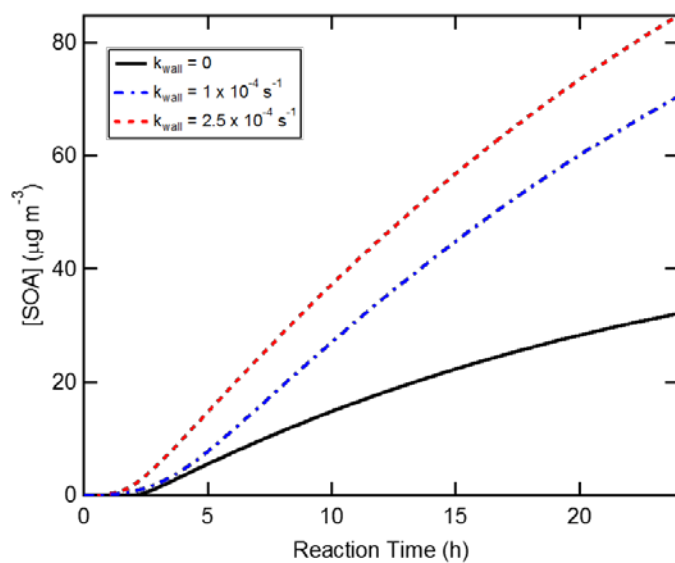
Figure S1. Box model simulations of SOA formation using SOM parameters determined from fitting low-NO_x toluene + OH SOA data assuming k_{wall} = 0, 1 x 10^{-4} and 2.5 x 10^{-4} s^{-1}, but where the simulations are run with k_{wall} = 0 s^{-1}. Reaction conditions here are [toluene]$_{t=0}$ = 100 μg m^{-3} and [OH] = 2 x 10^6 molecules cm^{-3}.

1
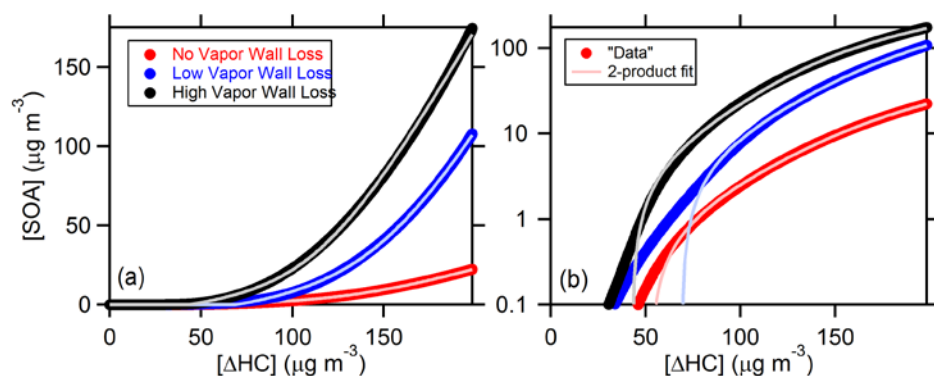
Figure S2. Example of 2-product fitting to SOA yield curves for dodecane + OH SOA formed under low-NO$_x$ conditions. The 2-product model was fit to simulated vapor wall-loss-corrected yield curves (circles) that were generated using the SOM model. The original SOM fits were performed using variable k_{wall} values to account for vapor wall losses, but the subsequent simulated yield curves were generated with k_{wall} = 0. The lines are colored according to the wall-loss condition used when SOM was fit to the chamber observations, no wall loss (red), low wall loss (blue) and high wall loss (black).The best 2-product fits are shown as solid lines. Panel (a) shows the curves and fits on a linear scale and panel (b) shows the same on a log scale. Note that on a linear scale the deviations between the fit curves and the "data" at low [SOA] is not visibly evident.
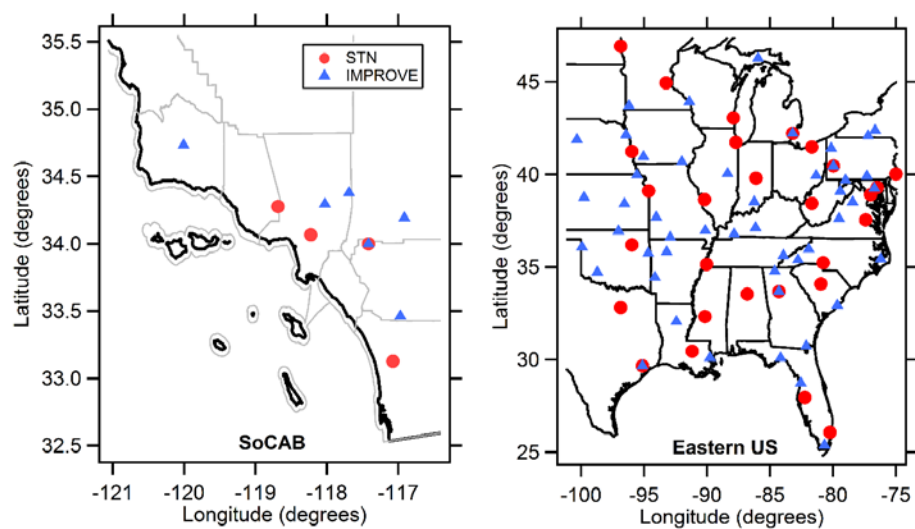
Figure S3. Map of STN and IMPROVE sites in the (left) SoCAB and (right) eastern US. STN sites are shown as red circles and IMPROVE sites as blue triangles.
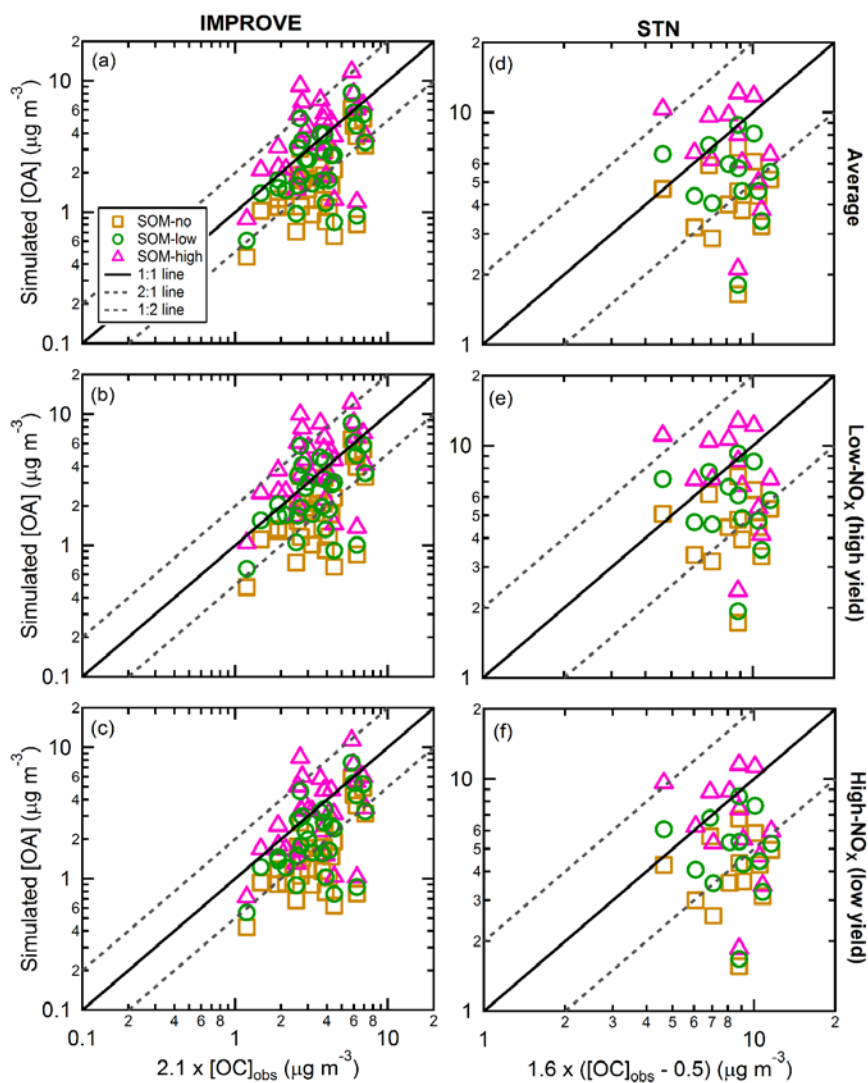
Figure S4. Scatter plots of simulated versus observed total OA (SOA + POA) concentrations for SoCAB for (left panels) IMPROVE and (right panels) STN sites. Simulation results are shown for SOM-no (orange), SOM-low (green) and SOM-high (pink). Results are reported from simulations run using the (top) average, (middle) low-NO$_x$ / high-yield, and (bottom) high-NO$_x$ / low-yield parameterizations.
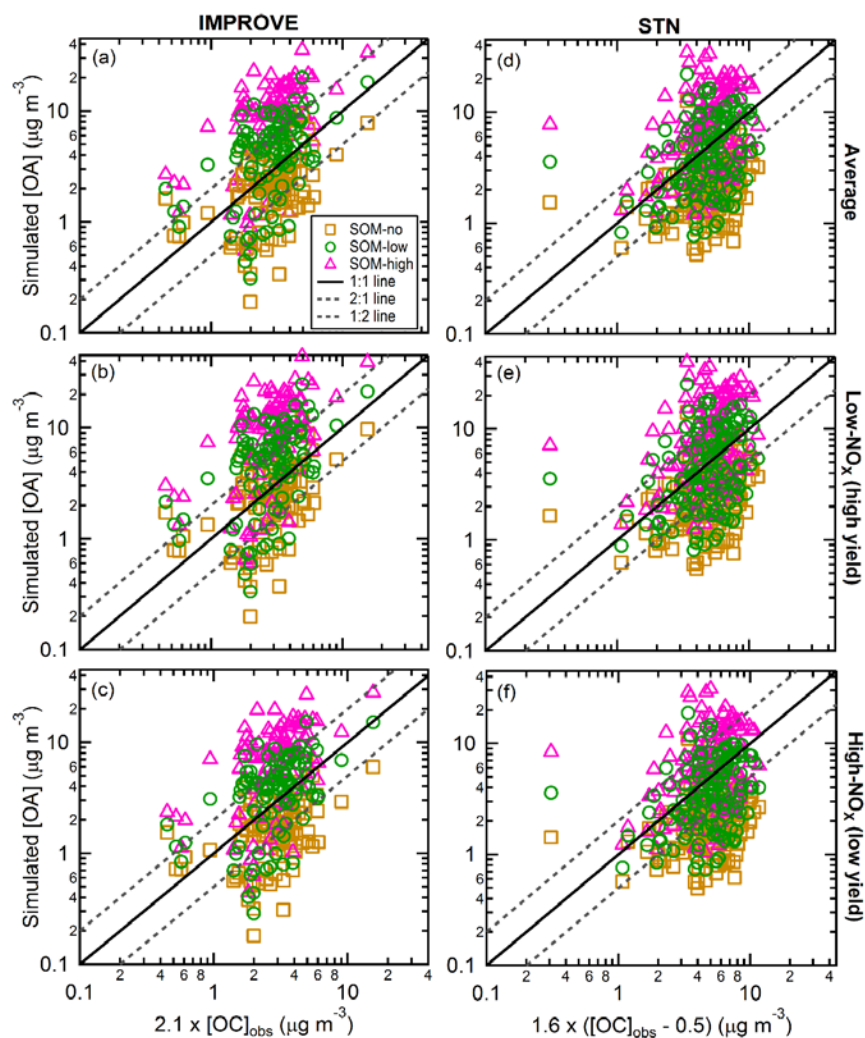
4

Figure S5. Scatter plots of simulated versus observed total OA (SOA + POA) concentrations for SoCAB for (left panels) IMPROVE and (right panels) STN sites. Simulation results are shown for SOM-no (orange), SOM-low (green) and SOM-high (pink). Results are reported from simulations run using the (top) average, (middle) low-NO$_x$ / high-yield, and (bottom) high-NO$_x$ / low-yield parameterizations. Only every other data point (one-in-two) is shown for visual clarity.

5

Table S1. List of best-fit SOM parameters determined by fitting SOM to experimental observations of SOA formation in the Caltech environmental chamber assuming that $k_{wall} = 1 \times 10^{-4}$ s^{-1} or 2.5×10^{-4} s^{-1}.

VOC Precursor Class	SAPRC-11 Species Name	VOC Surrogate	NO$_x$	m_{frag}	ΔLVP	p_{1O}	p_{2O}	p_{3O}	p_{4O}	Ref.[^]
				$k_{wall} = 1 \times 10^{-4}$ s^{-1}						
Long Alkanes	ALK5[*]	dodecane	low	0.677	1.57	0.97	0.023	0.003	0.004	(Cappa et al., 2013; Loza et al., 2014)
			high	0.186	1.45	0.961	0.001	0.002	0.036	
Benzene	Benzene	benzene	low	0.01	2.31	0.324	0.001	0.607	0.068	(Ng et al., 2007)
			high	0.73	1.47	0.018	0.001	0.981	0.001	
Toluene	ARO1	toluene	low	0.843	1.70	0.066	0.001	0.106	0.827	(Zhang et al., 2014)
			high	5	1.37	0.865	0.001	0.065	0.069	
m-xylene	ARO2	m-xylene	low	0.236	1.97	0.001	0.123	0.8	0.075	(Ng et al., 2007)
			high	0.0389	1.46	0.001	0.001	0.905	0.093	
Isoprene	Isoprene	isoprene	low	0.01	2.20	0.097	0.13	0.748	0.025	(Chhabra et al., 2011)
			high	0.745	2.15	0.808	0.189	0.002	0.001	
Terpenes	TRP1/SESQ[+]	α-pinene	low	0.156	1.89	0.316	0.554	0.087	0.043	(Chhabra et al., 2011)
			high	0.0588	1.92	0.064	0.865	0.063	0.008	
				$k_{wall} = 2.5 \times 10^{-4}$ s^{-1}						
Long Alkanes	ALK5[*]	dodecane	low	2	1.83	0.999	0.001	0.001	0.001	(Cappa et al., 2013; Loza et al., 2014)
			high	0.266	1.47	0.965	0.001	0.002	0.032	
Benzene	Benzene	benzene	low	0.0807	1.97	0.637	0.001	0.002	0.360	(Ng et al., 2007)
			high	0.824	1.53	0.008	0.001	0.991	0.001	
Toluene	ARO1	toluene	low	1.31	1.77	0.185	0.001	0.002	0.812	(Zhang et al., 2014)
			high	4.61	1.42	0.856	0.001	0.002	0.141	
m-xylene	ARO2	m-xylene	low	1.08	2.05	0.102	0.001	0.878	0.019	(Ng et al., 2007)
			high	0.0671	1.46	0.001	0.001	0.942	0.056	
Isoprene	Isoprene	isoprene	low	0.0839	2.44	0.096	0.379	0.518	0.007	(Chhabra et al., 2011)
			high	5	1.78	0.874	0.039	0.085	0.001	
Terpenes	TRP1/SESQ[+]	α-pinene	low	0.305	1.97	0.419	0.426	0.140	0.014	(Chhabra et al., 2011)
			high	0.16	1.91	0.500	0.422	0.070	0.008	

[^]These are the primary references for the experimental data. The data for the specific experiments used are presented in the supplemental material of (Zhang et al., 2014)

[*]For SOM, the ALK5 class is separated into long alkane species grouped according to carbon number. See (Jathar et al., 2015) for details.

[+]Although the same set of parameters are used to describe the formation of oxidation products and SOA from monoterpenes and sesquiterpenes, the SOA yield from sesquiterpenes is larger than for monoterpenes due to the larger number of carbon atoms comprising sesquiterpenes.

Table S2. Comparison between calculated non-fossil fractions of secondary organic aerosol (SOA) and secondary organic carbon (SOC).

Vapor Wall Loss Case	NO$_x$ condition	Central LA		Riverside	
		SOA	SOC	SOA	SOC
SOM-no	high-NO$_x$	0.27	0.24	0.28	0.25
	low-NO$_x$	0.44	0.41	0.40	0.37
SOM-low	high-NO$_x$	0.22	0.23	0.27	0.28
	low-NO$_x$	0.32	0.30	0.35	0.33
SOM-high	high-NO$_x$	0.22	0.25	0.28	0.31
	low-NO$_x$	0.33	0.32	0.37	0.36
		Atlanta		Smokey Mountains	
		SOA	SOC	SOA	SOC
SOM-no	high-NO$_x$	0.10	0.08	0.14	0.12
	low-NO$_x$	0.17	0.15	0.15	0.13
SOM-low	high-NO$_x$	0.19	0.18	0.27	0.27
	low-NO$_x$	0.18	0.17	0.22	0.20
SOM-high	high-NO$_x$	0.25	0.27	0.32	0.35
	low-NO$_x$	0.20	0.19	0.24	0.23

References

Cappa, C. D., Zhang, X., Loza, C. L., Craven, J. S., Yee, L. D., and Seinfeld, J. H.: Application of the Statistical Oxidation Model (SOM) to secondary organic aerosol formation from photooxidation of C12 Alkanes, Atmos. Chem. Phys., 13, 1591-1606, doi:10.5194/acp-13-1591-2013, 2013.

Chhabra, P. S., Ng, N. L., Canagaratna, M. R., Corrigan, A. L., Russell, L. M., Worsnop, D. R., Flagan, R. C., and Seinfeld, J. H.: Elemental composition and oxidation of chamber organic aerosol, Atmos. Chem. Phys., 11, 8827-8845, doi:10.5194/acp-11-8827-2011, 2011.

Jathar, S. H., Cappa, C. D., Wexler, A. S., Seinfeld, J. H., and Kleeman, M. J.: Multi-generational Oxidation Model to Simulate Secondary Organic Aerosol in a 3D Air Quality Model, Geosci. Model Dev., 8, 2553-2567, doi:10.5194/gmd-8-2553-2015, 2015.

Loza, C. L., Craven, J. S., Yee, L. D., Coggon, M. M., Schwantes, R. H., Shiraiwa, M., Zhang, X., Schilling, K. A., Ng, N. L., Canagaratna, M. R., Ziemann, P. J., Flagan, R. C., and Seinfeld, J. H.: Secondary organic aerosol yields of 12-carbon alkanes, Atmos. Chem. Phys., 14, 1423-1439, doi:10.5194/acp-14-1423-2014, 2014.

Ng, N. L., Kroll, J. H., Chan, A. W. H., Chhabra, P. S., Flagan, R. C., and Seinfeld, J. H.: Secondary organic aerosol formation from m-xylene, toluene, and benzene, Atmos. Chem. Phys., 7, 3909-3922, doi:10.5194/acp-7-3909-2007, 2007.

Zhang, X., Cappa, C. D., Jathar, S. H., McVay, R. C., Ensberg, J. J., Kleeman, M. J., and Seinfeld, J. H.: Influence of vapor wall loss in laboratory chambers on yields of secondary organic aerosol, Proc. Nat. Acad. Sci., 111, 5802-5807, doi:10.1073/pnas.1404727111, 2014.